THESIS FOR THE DEGREE OF LICENTIATE OF ENGINEERING

Energy Efficiency Comparison Between Two-level and Multilevel Inverters for Electric Vehicle Applications

Oskar Josefsson

Division of Electric Power Engineering
Department of Energy and Environment
CHALMERS UNIVERSITY OF TECHNOLOGY
Göteborg, Sweden 2013

Energy Efficiency Comparison Between Two-level and Multilevel Inverters for Electric Vehicle Applications

Oskar Josefsson

© Oskar Josefsson, 2013.
except where otherwise stated.
All rights reserved

Department of Energy and Environment
CHALMERS UNIVERSITY OF TECHNOLOGY
SE-412 96 Göteborg
Sweden
Telephone + 46 (0)31 772 00 00

To my family

Abstract

In order to contribute to the development of energy and cost efficient electric vehicles, a thorough analysis of two different electric converter topologies is performed, considering different drive cycles and different control strategies. In the electric vehicles available on the market today, a high voltage ($200-400\,V$) battery pack composed of several battery modules is connected to one or more inverters which create AC voltages to the electric propulsion machines. This thesis analyses the use of a modular battery-inverter concept, the cascaded multilevel inverter. Here, the battery modules have one inverter for each battery module, the inverters are then connected in series and controlled in order to create the AC voltages for the electric machines.

The simulation results shows that this concept lowers the inverter losses, mainly due to the possibility to use MOSFETs instead of IGBTs. The losses in the battery are on the other hand increased. If there was a possibility to filter out reactive power and harmonics from the battery (using input capacitors for each inverter), the drive train with the multilevel inverter will have lower losses than the two-level inverter for all the analysed driving cycles. If such filter capacitors can not be used, it is not beneficial to use the multilevel inverter for high speed driving cycles, such as the US06. For the more moderate new European driving cycle, the accumulated drive cycle losses in the battery and inverter are reduced by 25 % when using the multilevel inverter, even without filter capacitors, compared to the two-level inverter. Furthermore, when using infinitely large supporting capacitors in parallel to the battery modules, the loss reduction for the inverter and the battery becomes 72 % compared to the two-level inverter.

The multilevel inverter is able to control from which battery modules the energy is taken from, therefore the battery capacity is no longer limited by the weakest battery module. If one of the modules is damaged and the available energy is lower, the inverter can be controlled to utilize the remaining energy in the battery pack so the effect of the faulty module is not so severe. When using the propulsion inverter as a charger, the multilevel inverter also shows an increase in efficiency compared to the two-level inverter.

Keywords

Electric Vehicle (EV), Plug-in Electric Vehicle (PEV), Multilevel Inverter (MLI), Two-level Inverter (TLI), Integrated Charger, Drive Cycle, Efficiency.

Acknowledgement

The financial support from the Swedish Energy Agency is gratefully appreciated. I would like thank Robert Eriksson and Urban Kristiansson at Volvo-cars AB for interesting discussions and project leadership. I would also like to thank Lars Johannesson from the department of Signals and Systems for interesting inputs from a control perspective.

In the division, I would like to thank my supervisor and examiner Torbjörn Thiringer. The endless hours of discussions are extremely appreciated. Thank you! I would also like to thank Sonja Lundmark and Hector Zelaya De La Parra for their help with the project as co-supervisors and Anders Lindskog for the introduction of the project.

Working at the division of electric power engineering is a privilege, thank you all co-workers for making this such a nice environment to work in. I would like to aim a special thanks to my room mates David Steen and Saeid Haghbin. Your support and comments during the years have been extremely helpful, and fun. Thank you!

Finally I want to thank my family. Thank you for all the help and support. I am forever grateful!

Oskar Josefsson
Göteborg, February 2013

Contents

List of Nomenclatures

The following list presents nomenclatures that are used throughout this thesis:

V_{CE}	IGBT collector emitter voltage
I_C	IGBT collector current
$V_{t_{IGBT}}$	IGBT fixed voltage drop
$R_{on_{IGBT}}$	IGBT resistance
V_{DS}	MOSFET drain source voltage
I_D	MOSFET drain current
$R_{on_{MOSFET}}$	MOSFET resistance
T_{on}	Transistor turn on time
T_{off}	Transistor turn off time
V_{AC}	Diode anode cathode voltage
I_A	Diode anode current
$V_{t_{Diode}}$	Diode fixed voltage drop
R_{Diode}	Diode resistance
Q_{rr}	Diode reverse recovery charge
K_{rr}	Diode reverse recovery equivalent loss parameter
E_{RR}	Diode reverse recovery energy
V_{drr}	Diode voltage at reverse recovery

E_{on}	Transistor turn on energy
E_{off}	Transistor turn off energy
C	Capacitance of one MLI H-bridge input capacitor
n	Number of H-bridges for one phase in the MLI
N	Number of voltage levels one phase can produce
$V_{DC_{ML}}$	Input voltage for each H-bridge in the MLI
$V_{DC_{TL}}$	Input voltage for the TLI
$U_{phase_{RMSMAX}}$	Maximum phase voltage that can produced by the inverters
$U_{phase_{RMSMAXTHI}}$	Maximum phase voltage that can produced by the TLI when controlled with third harmonic injection
h	Harmonic number
$U_{ML}(h)$	Harmonic value at harmonic h for the MLI
α_1	Angle where the first H-bridge is turned on
α_2	Angle where the second H-bridge is turned on
α_3	Angle where the third H-bridge is turned on
$V_{out}(t)$	Inverter reference output voltage
$\hat{U}$	Amplitude of inverter reference output voltage
ω	Frequency of inverter reference output voltage
φ	Phase difference of inverter output voltage and current
a	Magnitude of third harmonic component
$\hat{I}$	Amplitude of inverter output current
f_{fund}	Frequency of inverter reference output voltage
T_f	Time period of inverter reference output voltage
f_{sw}	Switching frequency of the TLI

m_a	Modulation index
$D(t)$	Duty cycle of the TLI
$P_{cond_{IGBT_{1H}}}$	Conduction losses for the upper transistor in the TLI
$P_{cond_{IGBT_{1L}}}$	Conduction losses for the lower transistor in the TLI
$P_{cond_{Diode_{1H}}}$	Conduction losses for the upper diode in the TLI
$P_{cond_{Diode_{1L}}}$	Conduction losses for the lower diode in the TLI
$P_{conduction_{IGBTs_1}}$	Average conduction losses for the transistors in one leg in the TLI
$P_{conduction_{Diodes_1}}$	Average conduction losses for the diodes in one leg in the TLI
$P_{switch_{IGBT_{1H}}}$	Switching losses for the upper transistor in the TLI
$P_{switch_{IGBT_{1L}}}$	Switching losses for the lower transistor in the TLI
$P_{rr_{Diode_{1H}}}$	Switching losses for the upper diode in the TLI
$P_{rr_{Diode_{1L}}}$	Switching losses for the lower diode in the TLI
$P_{switch_{IGBTs_1}}$	Average switching losses for the transistors in one leg in the TLI
$P_{rr_{Diodes_1}}$	Average switching losses for the diodes in one leg in the TLI
$P_{Loss_{TLI}}$	Average total loss in the TLI
V_{drop}	Phase voltage drop in the MLI
$P_{conduction_{MLI}}$	Conduction losses for the MLI
$E_{on_{\alpha_{1...6}}}$	Turn on energy at switching instance 1 to 6
$E_{off_{\alpha_{1...6}}}$	Turn off energy at switching instance 1 to 6
$E_{rr_{\alpha_{1...6}}}$	Reverse recovery energy at switching instance 1 to 6
$P_{switch_{MLI}}$	Average switching losses in the MLI
$P_{Loss_{ML}}$	Average total loss in MLI

u_{sd}	Stator voltage in d-direction
u_{sq}	Stator voltage in q-direction
i_{sd}	Stator current in d-direction
i_{sq}	Stator current in q-direction
ψ_m	Magnetic flux density
p	Pole pairs
R_s	Stator resistance
L_d	Inductance in d-direction
L_q	Inductance in q-direction
$U_{phase_{RMS}}$	Machine phase voltage
$I_{phase_{RMS}}$	Machine phase current
$\angle\vec{u_s}$	Angle of machine voltage relative to machine position
$\angle\vec{i_s}$	Angle of machine current relative to machine position

Chapter 1

Introduction

1.1 Background

The automotive manufacturers are going through a time with introduction of many new technologies due to the increasing interest of electrified vehicles (EVs). A very important problem the car industry experiences is to utilize the energy in the battery in the most efficient way, but also to take care of the losses in the battery, the power electronics and the electrical machine. The power electronics must be designed and controlled in the most efficient way to be able to utilize this energy to achieve the longest driving distance for a given battery size. The importance of choosing the right power electronics in an EV is discussed in [1] and is stated to be of high importance to make the vehicle competitive. A problem today is that if one part of either the power electronic system or the battery is damaged, the whole system capacity is reduced to the capacity of this component. If one of these components fail, the car will not be able to continue to operate.

To be able to minimize the electric losses in the drive train, accurate models are needed. In order to adequately utilize such a model of the electric power train, some parts of vehicle modeling must also be included. Without finding the appropriate voltages, currents and phase angles, the losses in an inverter can not be determined. In [2] and [3] some simulation aspects special to EVs are shown, dealing with both the physical behaviour as well as the electrical one. It is shown that even though it is important to analyse the efficiency of each component, the different components determine the operation points for each other and therefore the complete drive train must be incorporated in the vehicle efficiency analysis.

The losses in the vehicle are not only dependent on the components chosen for the vehicle, the control strategies are also of high importance. This is

shown by [4] and [5] with a focus on that information about how the vehicle is used, affects the optimal control strategies. In reference [6] it is shown that accurate models of the losses and the operation points of the different components are of high importance in order to achieve the correct results. Since the electric machine in an EV runs at a large range of operating points, instead of analysing a single or a few operating points, it is important to consider different complete drive cycles, especially when the machine is used in the field weakening area. It is also vital that the models are verified against measurements and/or empirical data, other models and analytical calculations.

To be able to compare how good an electric vehicle drive train is, test procedures are needed. Different test procedures for EVs are explained in [7] where it is stated that one problem for making accurate testing is to describe equivalent fuel consumptions for an electric vehicle since other vehicles are measured in liters of fossil fuel per kilometer. In order to compare different electric drive trains, equivalent fuel consumption is of less importance, since the minimization of the losses for the same drive cycle leads to the best fuel consumption.

To make an EV competitive, the main goal is to develop a product that is economical. To be able to make an economical model it is important to have good price information about the components. Reference [8] shows an economical model that predicts the price of the components in EVs to decrease. However, they are also showing that the model is very uncertain which makes the analysis of the economical aspects of different drive trains problematic.

A state of the art analysis of the vehicles on the market today is needed in order to compare different EV setups. References [9] and [10] show an investigation of the market, and it is stated that the power electronics of the current generation of electric vehicles utilises similar power electronic concepts; the two-level inverter (TLI). It indicates that an increase of the research in power electronics for EVs is expected. In [11], a general study of the future of EVs is conducted. They expect that the power electronic technology is to play a very large role to meet the challenge of developing competitive EVs. In [12] and [13] the special requirements of power electronics in EVs are discussed and the challenges of choosing the optimal power electric component for an inverter to be used in EVs are explained. Different packages, for example, give different advantages in terms of cooling. In EVs, as mentioned before, the TLI is the far most used power electronic converter today. It uses six power electronic switches to create the voltage needed for an electrical machine, see Fig. 2.1. Due to the demand of a high voltage level, IGBTs are often used. The IGBTs have relatively high losses compared

to MOSFETs at this power level, so it would be beneficial to be able to use the MOSFET technology. One way to be able to use MOSFETs is to divide the battery to smaller units with lower voltage, and use one inverter for each battery module. The outputs of the inverters are then series connected to be able to create the voltage magnitude that the electric machine requires. This inverter is called a cascaded multilevel inverter (MLI) and can be seen in Fig. 2.2.

The plug-in electric vehicle, PEV, and the plug-in hybrid electric vehicle, PHEV, must have a charger to be able to charge the battery from the grid. In the great majority of the electrical vehicles out on the market today, the charger is a stand-alone component. It can be either an on-board charger that is located in the vehicle, or it can be an off-board charger located at different locations in the infrastructure. It is advantageous if the propulsion power electronics can be used also for charging; then the separate power electronics in the on board charger is not needed, and space as well as cost can be reduced. This works fine with the TLI, see [14], however, the consequences when doing the same with the MLI, is not yet compared for a vehicle application.

The advantages and benefits of using a MLI in an electrified vehicle are discussed in [15] and in [16]. It is stated that the MLI has almost no electromagnetic interference (EMI) and therefore a safer and more accessible choice to have in a vehicle. The efficiency is discussed in general terms, but is calculated to be higher than the TLI.

Obviously the MLI has advantages regarding EMI and battery utilisation, however, a traceable result of the benefits from an energy point of view to use a MLI in electrified vehicles, and to what extent, is missing.

1.2 Purpose of work

The purpose of this work is to analyse the opportunities of using a MLI in an electric powered vehicle. The main focus is made on the energy efficiency when using different drive cycles and control strategies. To quantify the electric energy benefits for various drive cycles is accordingly a vital theme. In order to analyse the inverter, it is important to incorporate a relevant electrical machine so that the appropriate inverter operating conditions are met. However, the economical aspects are not dealt with.

1.3 Contributions

According to the author the following contributions have been made with this thesis.

- Quantified the losses in an electric power train for the MLI, and put it in relation to the losses in a TLI.
- Analysed the electrical losses for different driving cycles to be able to determine when it is beneficial to use a MLI.
- Developed an analytical formula for the losses of a TLI controlled with third harmonic injection.
- Demonstrated that the losses are very sensitive to the control angles α_1, α_2 and α_3 for the MLI.
- Experimentally showed the possibility to balance the battery groups.
- Experimentally verified the battery current waveforms from a MLI.

Chapter 2

Drive system topologies and loss modeling

This chapter derives mathematical models that describes the losses in the electric power train as a function of how the vehicle is operated and which control strategies that are used.

2.1 Converter topologies

Two different inverter topologies will be studied in this thesis, the cascaded multilevel inverter (MLI) and the classical two-level inverter (TLI).

2.1.1 Two-level inverter (TLI)

The TLI is by far the most common inverter used in electrified vehicles. It consists of six switches divided into three legs, see Fig. 2.1. An anti-parallel diode is placed in parallel to each switch to allow current to flow in the reverse direction as well. The battery is connected to the input of the inverter supplying it with a voltage level of $V_{DC_{TL}}$. The inverter can produce eight different states depending on the control of the six switches.

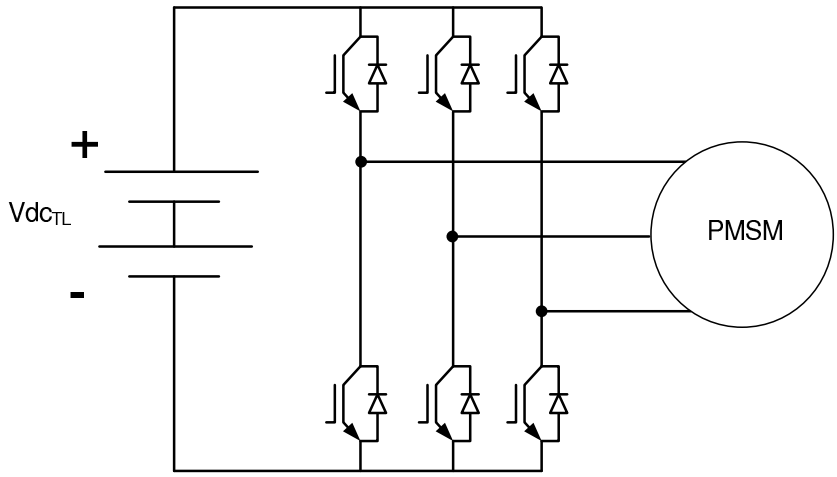

Figure 2.1: Topology of a two-level inverter (TLI)

2.1.2 Multilevel inverter (MLI)

A multilevel inverter can be built up using many different topologies. The one analysed in this thesis is the cascaded multilevel inverter, see Fig. 2.2. It consists of series connected H-bridges which can be controlled independently. Every H-bridge has a separate energy storage with a voltage of $V_{DC_{ML}}$ attached to it and by controlling the switches in the H-bridge in different ways, one bridge can create $V_{DC_{ML}}$, $-V_{DC_{ML}}$, 0 and open circuit, to its output. Since many H-bridges are connected in series the total voltage can vary in several steps. If the voltage sources are equal, the number of voltage levels, N, becomes

$$N = 2n + 1 \tag{2.1}$$

where n is the number of H-bridges for each phase.

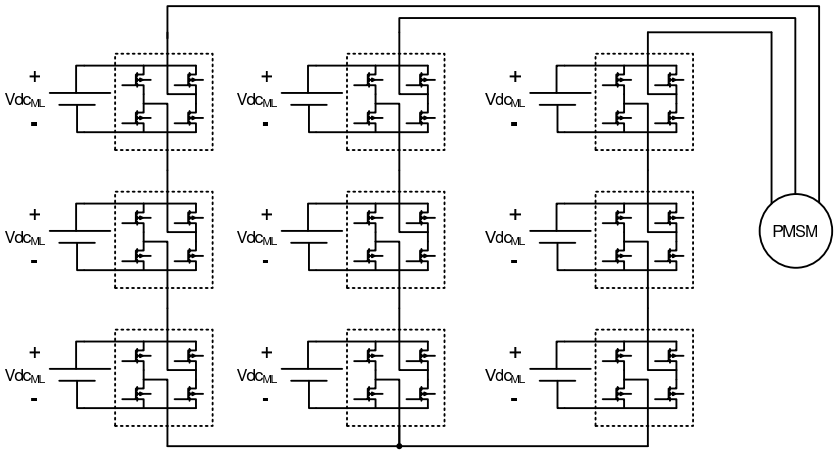

Figure 2.2: Topology of a 7-level multilevel inverter (MLI)

2.2 Power electronic components and their losses

To be able to calculate the losses in different inverter topologies, information about the components are needed. In the TLI, IGBTs are used due to their high voltage blocking ability, see Fig. 2.3b, together with diodes, see Fig. 2.3c. In the MLI, MOSFETs will be used due to the lower blocking voltage requirement in the MLI, see Fig. 2.3a. A MOSFET has a built in body diode that sometimes is sufficient. In this thesis, this is the case, so no external diodes will be used in this analysis.

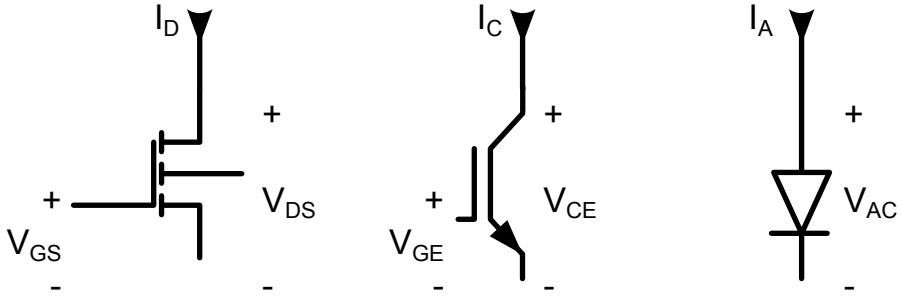

(a) MOSFET (b) IGBT (c) Diode

Figure 2.3: Power electronic components

2.2.1 IGBT

The losses in an IGBT are described in [17] when used in a bridge configuration. It is often assumed that the voltage drop of the IGBT is approximated

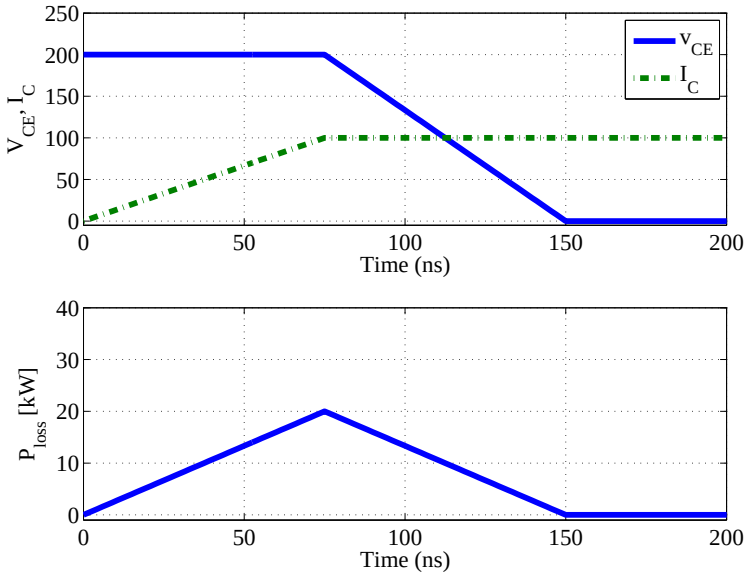

Figure 2.4: Turn on losses for an IGBT, times approximated for a 600 V IGBT

with two linear lines when it is turned on. The two lines are expressed as

$$\begin{aligned} V_{CE}(I_C) &= V_{t_{IGBT}} + R_{on_{IGBT}} I_C & I_C &> 0 \\ I_C &= 0 & V_{CE} &< V_{t_{IGBT}} \end{aligned} \tag{2.2}$$

where $R_{on_{IGBT}}$ is the resistance when fully turned on, $V_{t_{IGBT}}$ is the constant voltage drop in the IGBT, I_C is the current through the IGBT and V_{CE} is the voltage over the IGBT.

When turned off the IGBT is described as

$$I_C = 0. \tag{2.3}$$

The switching losses for an IGBT are due to that it takes time to increase and decrease the current through and voltage on the switch. This loss can (a bit idealized) be described as seen in Fig. 2.4.

The energy loss at turn on is then for this simplified case calculated with

$$E_{on}(V_{CE}, I_C) = \int_0^{T_{on}} I_C(t) V_{CE}(t)\, \mathrm{d}t = \frac{V_{CE} I_C T_{on}}{2} \tag{2.4}$$

where T_{on} is the time to fully turn on the IGBT.

The energy loss at turn off will in the same way be equal to

$$E_{off}(V_{CE}, I_C) = \int_0^{T_{off}} I_C(t)V_{CE}(t)\,\mathrm{d}t = \frac{V_{CE}I_C T_{off}}{2} \tag{2.5}$$

where T_{off} is the time to fully turn of the IGBT.

However, in reality the switching losses can not be accurately predicted using algebraic expressions, even using more complexity. Therefore, if more accurate results are needed, tables from the data sheets are commonly used.

Observe that in order to find the parameters that describe this loss, the data sheet of the component is used.

2.2.2 MOSFET

The losses of a MOSFET used in bridge configuration is described in [18]. By supplying a voltage between the gate and the source, the MOSFET transistor turns on and is assumed to behave purely resistive. The voltage drop of a turned on MOSFET transistor is therefore approximated with a linear line as

$$V_{DS}(I_{DS}) = R_{on_{MOSFET}} I_D \tag{2.6}$$

where $R_{on_{MOSFET}}$ is the resistance in the MOSFET when turned on, I_{DS} is the current through the MOSFET and V_{DS} is the voltage over the MOSFET.

When no voltage is supplied to the gate, the MOSFET is turned off and the MOSFET then blocks the current very well. Due to the physics of the MOSFET technology there is always an antiparallel diode (body diode) which will start to conduct when the MOSFET has a negative voltage applied over it. When a negative current flows through the component, the current will go through the "parasitic/inherent body diode" if no gate voltage is supplied. By turning on the MOSFET when a negative current is flowing in the MOSFET, the voltage drop is reduced. The current will then flow through the channel instead of the body diode and the losses are decreased.

The switching losses for a MOSFET are due to the rise and fall time of both the current through and the voltage over the component. This loss can (again a bit idealized) be described as seen in Fig. 2.5. The energy loss at turn on is then calculated by

$$E_{on}(V_{DS}, I_D) = \int_0^{T_{on}} I_D(t)V_{DS}(t)\,\mathrm{d}t = \frac{V_{DS}I_D T_{on}}{2} \tag{2.7}$$

where T_{on} is the time to fully turn on the MOSFET.

The energy loss at turn off will in the same way be equal to

$$E_{off}(V_{DS}, I_D) = \int_0^{T_{off}} I_D(t) V_{DS}(t)\,\mathrm{d}t = \frac{V_{DS} I_D T_{off}}{2} \tag{2.8}$$

where T_{off} is the time to fully turn off the MOSFET.

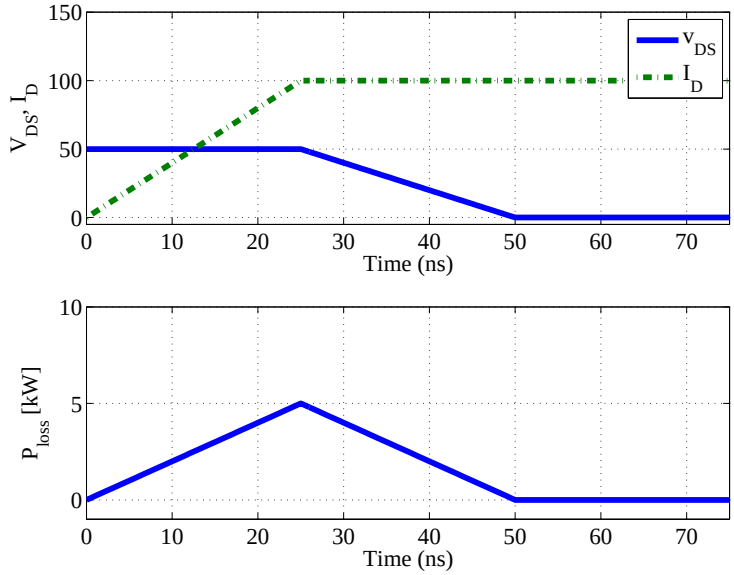

Figure 2.5: Turn on losses for MOSFET, times approximated for a 100 V IGBT

2.2.3 Diode

The losses of a diode used in a bridge configuration is discussed in both [17] and in [18]. The voltage drop of the diode is approximated with two linear lines as

$$\begin{aligned} V_A(I_A) &= V_{t_{Diode}} + R_{Diode} I_A & I_A &> 0 \\ I_A &= 0 & V_A &< V_{t_{Diode}} \end{aligned} \tag{2.9}$$

where R_{Diode} is the resistance in the diode, $V_{t_{Diode}}$ is the constant voltage drop in the Diode, I_{AC} is the current through the diode and V_{AC} is the voltage over the Diode.

The switching loss of a diode is assumed to be zero at turn on and turn off, but at turn off the diode has to deplete the charges that are stored in the junction from when it vas forward biased. This will create a current in the

reverse direction for a short period of time and the energy that is released becomes a loss in both the diode and the opposing switch when connected in a leg configuration. The charge that has to be depleted is current dependent and is for simplicity assumed to be proportional to the current that flew in the diode at the instant right before turn off. The total energy loss can according to [17] be written as

$$E_{RR} = \frac{Q_{rr} V_{drr}}{4} = \frac{Q_{rr}(-V_{AC})}{4} = K_{rr}(-V_{AC}) I_A. \tag{2.10}$$

where Q_{rr} is the charge stored in the diode at the time of reverse recovery and K_{rr} is the loss factor. The loss factor K_{rr} is taken from the data sheet where the reverse recovery loss is often specified at a certain blocking voltage and current.

Again, in reality, E_{RR} is a complicated parameter to determine and data sheets values with non-linear relations are typically used.

2.2.4 Miscellaneous power electronic components

Driver circuit

The driver circuit for the transistors is assumed to be lossless compared to the energy supplied to the electrical machine and is therefore neglected.

Capacitors

The losses in the capacitors are neglected in this thesis. It is assumed that the battery loss is much higher.

2.3 Modulation strategies

2.3.1 Two-level inverter

PWM

When a TLI is controlled in sub-oscillating PWM-mode, three voltage references are created. These references are compared to a triangular wave with a frequency equal to the switching frequency. When the reference is higher than the triangular wave, the upper side switch in that leg is activated (turned on), otherwise the lower side switch is activated. Actually, it is possible to use something called over modulation, where the reference wave is above the triangular wave. However, this will cause low-frequency harmonics which are hard to filter away. In this thesis, over modulation is not considered for simplicity and noise reasons. A margin of 10% is set on the output voltage to guarantee controllability of the current, to provide a minimum on and off time of the modules, and to account for the blanking time and the losses in the inverter. The maximum phase motor voltage will then be equal to

$$U_{phase_{RMSMAX}} = 0.9\frac{V_{DC_{TL}}}{2\sqrt{2}}. \tag{2.11}$$

There are also other methods to find the switching instances such as DTC.

Third harmonic injection(THI)-PWM

When a TLI is controlled in THI-PWM-mode three voltage references are created and compared to a triangular wave with a frequency equal to the switching frequency in the same way as in the PWM strategy. By adding a third harmonic, the neutral point of the machine is altered up and down. The machine will not react to this third harmonic since it is a three phase system without the neutral point of the machine connected to the inverter neutral point. The advantage is that the DC-bus voltage can be utilized to a higher extent. A margin of 10% is utilized on the output voltage to guarantee controllability of the current. The maximum phase motor voltage, with "low-harmonic" free voltages, will then be equal to

$$U_{phase_{RMSMAXTHI}} = 0.9\frac{V_{DC_{TL}}}{\sqrt{3}\sqrt{2}} \tag{2.12}$$

which is about 15 % higher than the PWM strategy. This is the voltage level that will be used in this thesis.

In order to describe the phase voltage used, the modulation index m_a is typically utilised. For the two-level inverter the modulation index m_a is defined according to

$$U_{phase} = m_a \frac{V_{DC_{TL}}}{\sqrt{3}\sqrt{2}} \tag{2.13}$$

where m_a can go up to 1.0 without entering over modulation.

Running the inverter with THI-PWM will give a duty cycle D (the ratio of the active time between the upper and lower transistor in the leg) according to

$$D(t) = 0.5 + \frac{U_{out}(t)}{V_{DC_{TL}}}. \tag{2.14}$$

2.3.2 Multilevel inverter

The MLI will be controlled with Fundamental Selective Harmonic Elimination, FSHE, see [19], [20]. By choosing when to turn on the different H-bridges in the MLI, the amplitude of the fundamental frequency as well as the harmonics are controlled. For a N-level inverter the amplitude of the fundamental frequency and $\frac{N-3}{2}$ number of harmonics can be controlled. Since the motor acts as a phase current low pass filter, it is of importance to minimize the lowest harmonics since these are less effectively filtered.

The waveform built up by the 7-level MLI analyzed in this thesis can be seen in Fig. 2.6. The angles α_1,α_2 and α_3 describe the instances when the H-bridges should be activated.

The fourier series expansion of the signal for the different harmonics, h, can be written as

$$U_{ML}(h) = \frac{4}{h\ \pi}[V_{DC_{ML}} cos(h\ \alpha_1) + V_{DC_{ML}} cos(h\ \alpha_2) + V_{DC_{ML}} cos(h\ \alpha_3)] \tag{2.15}$$

according to [19] when assuming that the DC-voltages are equal for all the H-bridges. Setting the amplitude of harmonic 5 and 7 to zero the equation system provides the switching angles for different amplitudes of the fundamental frequency and can be seen in Fig. 2.7. The modulation index can go up to 1.07 without loosing the control to eliminate the 5th and 7th harmonic. At modulation index below 0.5, the control over the harmonics are also lost but are minimized with a prioritization on the 5th harmonic. To keep the battery cells balanced, the controller makes sure to use the battery with the highest voltage as the the one controlled with α_1 and the one with the lowest voltage with α_3. The maximum voltage the inverter can produce with a margin of 10% can accordingly be expressed as

$$U_{phase_{RMS\ MAX}} = 0.9 \cdot 1.07 \frac{V_{DC_{ML}} \cdot n}{\sqrt{2}}. \tag{2.16}$$

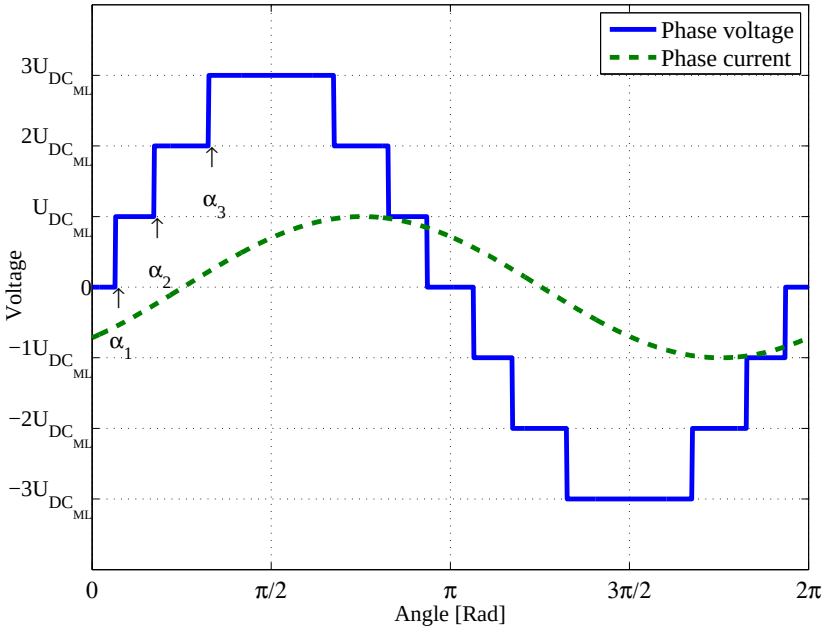

Figure 2.6: Phase voltage from 7-level MLI

For the MLI operated with FSHE the modulation index m_a is defined according to

$$U_{phase} = m_a \frac{V_{DC_{ML}} \cdot n}{\sqrt{2}} \tag{2.17}$$

where m_a can go up to 1.07 without loosing control over the cancelation of the low-frequency harmonics.

PWM

The MLI can operate in two kinds of PWM mode. One option is to create separate triangular waves for the different H-bridges and have one reference signal. In the other operation mode all levels are switched with the same control signal and uses one triangular wave. This results in an output voltage waveform identical to the TLI. The advantage of this control strategy is that the power is taken from all the batteries and therefore minimizes the losses in the batteries.

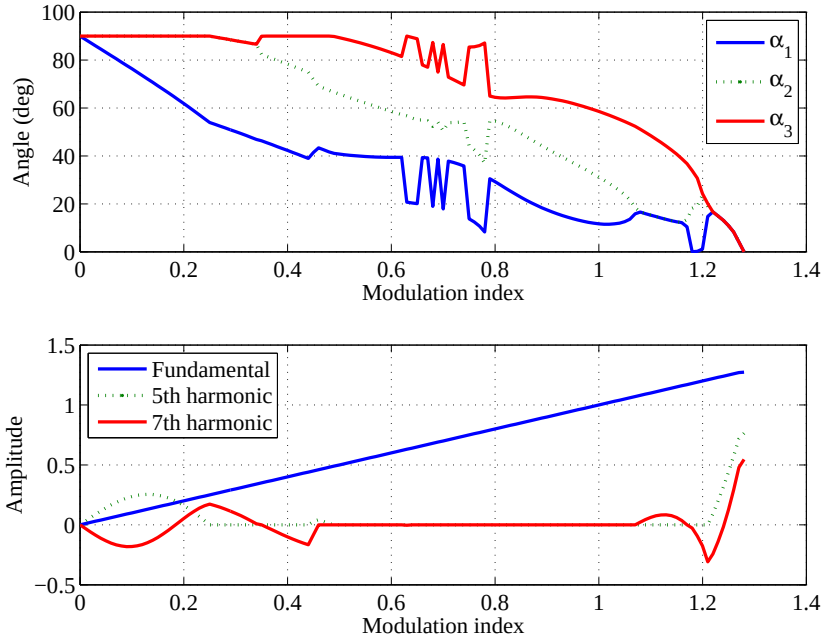

Figure 2.7: Switch angles and harmonics for different modulation indexes

2.4 Inverter loss modeling

2.4.1 Two level inverter (TLI)

To be able to calculate the losses in the TLI, information about the operating points used and the control strategy used is needed. The TLI will in this analysis be controlled with THI-PWM. The reference output voltage for the first phase is described as

$$V_{out}(t) = \hat{U}[\sin(\omega t + \varphi) + a\sin(3\omega t + 3\varphi)] \tag{2.18}$$

and the current as

$$I_{out}(t) = \hat{I}\sin(\omega t) \tag{2.19}$$

where $\hat{U}$ is the amplitude of the phase voltage, ω is the electric frequency, φ is the phase difference between voltage and current and $\hat{I}$ is the amplitude of the phase current. The amplitude of the third harmonic component a should be selected to 0.19 for maximum utilization of the DC-voltage, [21].

Conduction losses

The losses are calculated for one phase of the inverter and are then scaled to be valid for three phases. During the time when the current is positive,

the current will go through $IGBT_{1H}$ and $Diode_{1L}$, see Fig. 2.1. The losses in $IGBT_{1L}$ and $Diode_{1H}$ will be the same during the time when the current is negative. If the frequency of the sine wave is assumed to be much smaller than the switching frequency, the current and the reference voltage can be assumed to be constant during one switching period. The average conduction loss in $IGBT_{1H}$ and $Diode_{1L}$ can then be expressed as

$$P_{cond_{IGBT_{1H}}}(I_{out}, D) = \int_0^{T_{sw}} V_{DS}(I_D) I_D \, \mathrm{d}t = DI_{out}V_{t_{IGBT}} + DR_{on_{IGBT}}I_{out}^2 \quad (2.20)$$

and

$$P_{cond_{Diode_{1L}}}(I_{out}, D) = \int_0^{T_{sw}} V_{DS}(I_D) I_D \, \mathrm{d}t = (1-D)I_{out}V_{t_{Diode}} + (1-D)R_{on_{Diode}}I_{out}^2 \quad (2.21)$$

using (2.2) and (2.9).

To calculate the average conduction losses for one phase, one can choose to study the positive part of the current, knowing that the current only goes through $IGBT_{1H}$ and $Diode_{1L}$. Knowing that the same losses will be generated in $IGBT_{1L}$ and $Diode_{1H}$ during the negative part of the current, the average losses of one leg can then, by combining (2.20) and (2.14), be written as

$$P_{conduction_{IGBTs_1}} = \frac{\int_0^{T_f} P_{cond_{IGBT_{1H}}}(t) + P_{cond_{IGBT_{1L}}}(t) \, \mathrm{d}t}{T_f} = \frac{\int_0^{T_f/2} P_{cond_{IGBT_{1H}}}(t) \, \mathrm{d}t}{T_f/2} = \hat{I}V_{t_{IGBT}}(\frac{1}{\pi} + \frac{\hat{U}\cos\varphi}{2V_{DC_{TL}}}) + R_{on_{IGBT}}\hat{I}^2(\frac{1}{4} + \frac{4\hat{U}\cos\varphi}{3\pi V_{DC_{TL}}} - \frac{2a \cdot cos(3\varphi)}{15\pi}). \quad (2.22)$$

The losses in the diode can be calculated in the same way using (2.21)

and (2.14) which gives

$$P_{conduction_{Diodes_1}} = \frac{\int_0^{T_f} P_{cond_{Diode_{1H}}}(t) + P_{cond_{Diode_{1L}}}(t)\,\mathrm{d}t}{T_f} = \frac{\int_0^{T_f/2} P_{cond_{Diode_{1L}}}(t)\,\mathrm{d}t}{T_f/2} = \hat{I}V_{t_{Diode}}(\frac{1}{\pi} - \frac{\hat{U}\cos\varphi}{2V_{DC_{TL}}}) + R_{on_{Diode}}\hat{I}^2(\frac{1}{4} - \frac{4\hat{U}\cos\varphi}{3\pi V_{DC_{TL}}} + \frac{2a\cdot cos(3\varphi)}{15\pi}). \quad (2.23)$$

Switching losses

The switching losses for the IGBTs can be calculated with the assumption that the fundamental frequency is much lower than the switching frequency. If the leg would operate in DC-mode, the average switching loss for $IGBT_{1H}$ can be described as

$$P_{switch_{IGBT_{1H}}}(I_{out}) = [E_{on}(I_{out}) + E_{off}(I_{out})]f_{sw} = \frac{(T_{on}+T_{off})V_{DC_{TL}}I_{out}f_{sw}}{2}. \quad (2.24)$$

For the diodes, the turn on and turn off losses are neglected but the reverse recovery can have a significant contribution to the losses. It can be written as

$$P_{rr_{Diode_{1L}}}(I_{out}) = E_{rr}(I_{out})f_{sw} = K_{rr}V_{DC_{TL}}I_{out}f_{sw} \quad (2.25)$$

using (2.10).

Operating the converter in AC mode, the switch losses for the IGBTs in one leg can then be calculated as

$$P_{switch_{IGBTs_1}} = \frac{\int_0^{T_f/2} 2\frac{(T_{on}+T_{off})V_{DC_{TL}}I_{out}(t)f_{sw}}{2}\,\mathrm{d}t}{T_f} = \frac{2(T_{on}+T_{off})V_{DC_{TL}}f_{sw}\hat{I_{out}}}{\pi} \quad (2.26)$$

and the diode losses as

$$P_{rr_{Diodes_1}} = \frac{\int_0^{T_f/2} 2K_{rr}V_{DC_{TL}}I_{out}(t)f_{sw}\,\mathrm{d}t}{T_f} = \frac{2K_{rr}V_{DC_{TL}}\hat{I_{out}}f_{sw}}{\pi}. \quad (2.27)$$

Total losses

The total losses for a TLI running in AC-mode then becomes the sum of the losses in one leg times the number of legs which gives

$$P_{Loss_{TLI}} = 3(P_{conduction_{IGBTs_1}} + P_{conduction_{Diodes_1}} + P_{switch_{IGBTs_1}} + P_{rr_{Diodes_1}}) \quad (2.28)$$

using (2.22), (2.23), (2.26) and (2.27).

2.4.2 Multilevel inverter (MLI)

To be able to calculate the losses in the MLI, information about the operating point is needed as well as the control strategy. It will be controlled with Fundamental Selective Harmonic Elimination, FSHE. The MLI is assumed to be operating at an output voltage expressed as

$$V_{out}(t) = \hat{U}(\sin(\omega t + \varphi)) \tag{2.29}$$

and the current as

$$I_{out}(t) = \hat{I}\sin(\omega t). \tag{2.30}$$

Conduction losses

The current will always go through two transistors for each H-bridge. The voltage drop for one MOSFET can be written according to (2.6). The total voltage drop will therefore be equal to

$$V_{drop} = 2nI_{out}(t)R_{on_{MOSFET}} \tag{2.31}$$

independently of the current direction assuming that the MOSFET is turned on when conducting in the reverse direction.

The conduction power loss for all three phases of the MLI can therefore be calculated as

$$P_{conduction_{MLI}} = 6nI^2_{out_{RMS}}R_{on_{MOSFET}} = 3n\hat{I}^2R_{on_{MOSFET}}. \tag{2.32}$$

Switching losses

The switching losses can be described as a sum of the energy losses during one cycle. When controlled with FSHE, the switching occurs very seldom, see Fig. 2.6. During the first three switching instances, the inverter switches the H-bridges to create a positive voltage. Depending on the current direction this will result in either a turn on or a turn off loss. The loss for the MOSFET and diode can therefore at the first three switching instances be written as

$$\begin{aligned} E_{on_{\alpha_{1,2,3}}} &= \frac{V_{dc_{ML}}I(\alpha_{1,2,3})T_{on}}{2} && I(\alpha_{1,2,3}) \geq 0 \\ E_{on_{\alpha_{1,2,3}}} &= 0 && I(\alpha_{1,2,3}) < 0 \end{aligned} \tag{2.33}$$

$$\begin{aligned} E_{off_{\alpha_{1,2,3}}} &= 0 && I(\alpha_{1,2,3}) \geq 0 \\ E_{off_{\alpha_{1,2,3}}} &= \frac{V_{dc_{ML}}I(\alpha_{1,2,3})T_{off}}{2} && I(\alpha_{1,2,3}) < 0 \end{aligned} \tag{2.34}$$

$$\begin{aligned} E_{rr_{\alpha_{1,2,3}}} &= V_{dc_{ML}}I(\alpha_{1,2,3})K_{rr} && I(\alpha_{1,2,3}) \geq 0 \\ E_{rr_{\alpha_{1,2,3}}} &= 0 && I(\alpha_{1,2,3}) < 0. \end{aligned} \tag{2.35}$$

For the fourth, fifth and sixth switching instances the inverter switches to create zero volts for the inverters. This gives a loss according to

$$E_{on_{\alpha_{4,5,6}}} = 0 \qquad I(\alpha_{4,5,6}) \geq 0$$

$$E_{on_{\alpha_{4,5,6}}} = \frac{V_{dc_{ML}} I(\alpha_{4,5,6}) T_{on}}{2} \qquad I(\alpha_{4,5,6}) < 0 \tag{2.36}$$

$$E_{off_{\alpha_{4,5,6}}} = \frac{V_{dc_{ML}} I(\alpha_{4,5,6}) T_{off}}{2} \qquad I(\alpha_{4,5,6}) \geq 0$$

$$E_{off_{\alpha_{4,5,6}}} = 0 \qquad I(\alpha_{4,5,6}) < 0 \tag{2.37}$$

$$E_{rr_{\alpha_{4,5,6}}} = 0 \qquad I(\alpha_{4,5,6}) \geq 0$$

$$E_{rr_{\alpha_{4,5,6}}} = V_{dc_{ML}} I(\alpha_{4,5,6}) K_{rr} \qquad I(\alpha_{4,5,6}) < 0. \tag{2.38}$$

During switching occasion 7 to 12 the losses will be equal to the loss during switch 1 to 6. Therefore the losses can be calculated as

$$P_{switch_{MLI}} = 3 \cdot 2 \cdot f_{fund} \sum_{n=1}^{6} (E_{on_{\alpha_n}} + E_{off_{\alpha_n}} + E_{rr_{\alpha_n}}). \tag{2.39}$$

Total losses

The total losses for the multilevel inverter can be written as

$$P_{Loss_{ML}} = P_{conduction_{MLI}} + P_{switch_{MLI}} \tag{2.40}$$

using (2.32) and (2.39).

2.5 Energy storage

In the literature many different models exists for describing the electrical behaviour of a battery. In [22] and [23] evaluations for some different battery models are discussed and tested. For electric vehicles a dynamic model described by time constants is proposed by [24]. In [25] a test model is proposed to try to make a general test procedure for batteries used in electrified vehicles to be able to make fair comparisons between different manufacturers and sorts.

2.5.1 Battery

The battery is modelled as a fixed voltage source with an internal resistance. When comparing the TLI and the MLI the same number of reference cells are used to give a fair comparison. They are combined in such a way that the two different inverters will be able to produce the same maximum voltage to the electric machine.

For the TLI the input capacitor of the inverter is assumed large enough to supply all the reactive power. The battery current is therefore assumed to be a constant current during steady state operation.

For the MLI the battery current is calculated for three cases. In the first case, no input capacitors are assumed. In the second case the inverter is assumed to have infinity large capacitors connected to the input of the H-bridges to smoothen out the battery current. In the third and last case the input capacitors have a value. The battery current waveform for the battery packs in phase one can be seen in Fig. 2.8, Fig. 2.9 and Fig. 2.10 for the case with infinity large capacitors and without capacitors. If a capacitor of 3.6 mF, same energy amount as a 0.5 mF capacitor on the high voltage TLI, is placed at the input and the inverter is operating at a fundamental frequency of 400 Hz, the battery current would be filtered forming the solid blue waveform seen in Fig. 2.11. Decreasing the current ripple decreases the battery losses since the RMS value decreases.

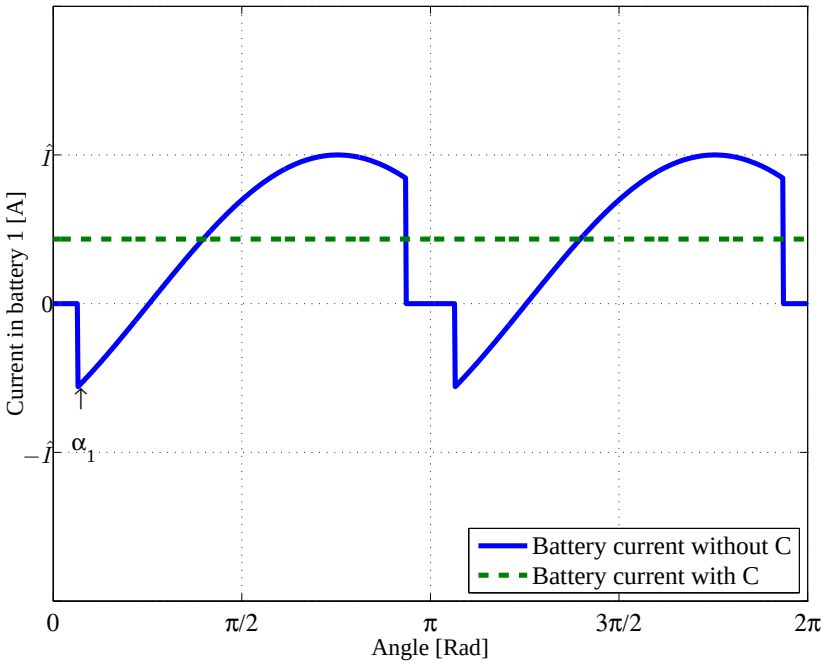

Figure 2.8: Current through the battery module controlled with α_1

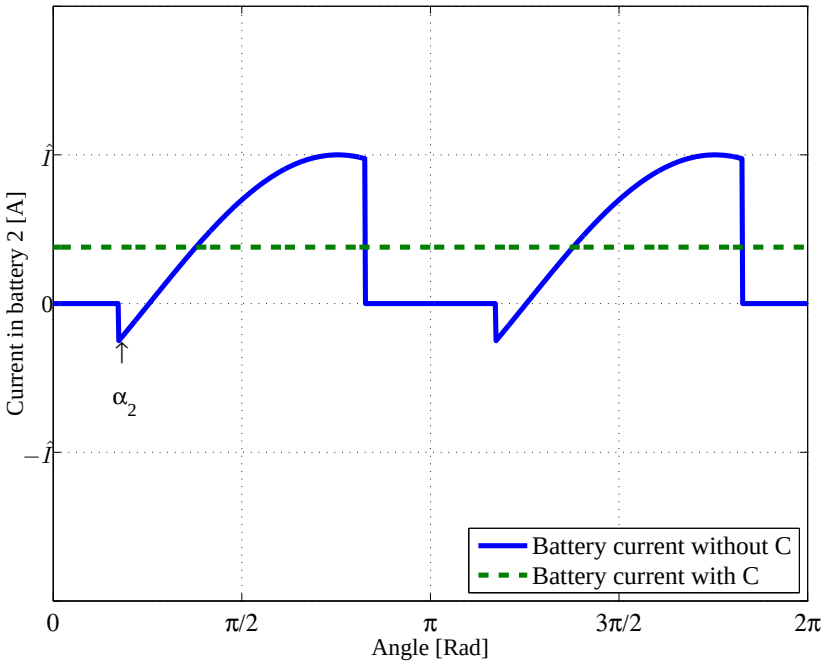

Figure 2.9: Current through the battery module controlled with α_2

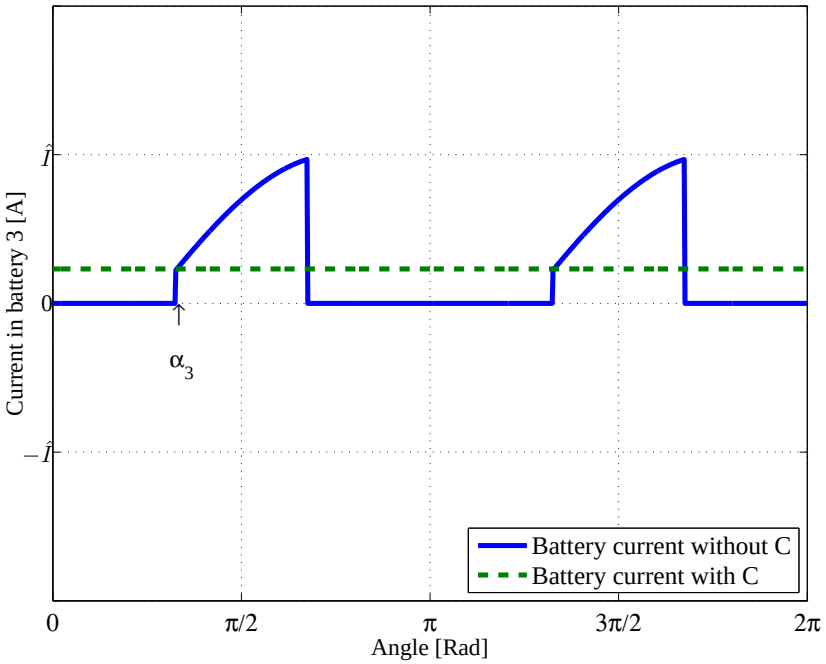

Figure 2.10: Current through the battery module controlled with α_3

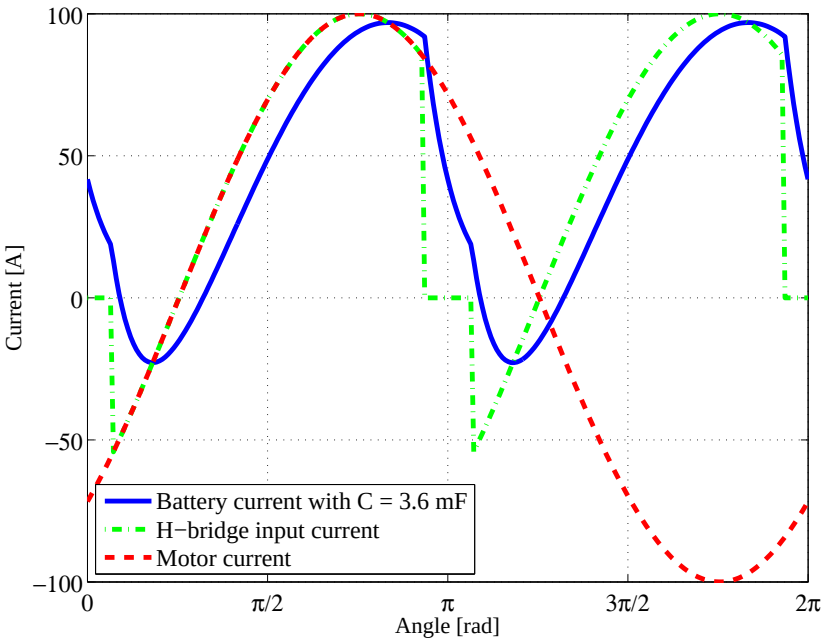

Figure 2.11: Current through the battery module controlled with α_1 and with an input capacitor of 3.6 mF

2.6 Electric machine and torque control

Many different electric machine topologies suitable for EVs exists. The switched reluctance machine, SRM, is discussed in [26] where it is stated that it can be a good choice for electrified vehicles, especially for high speeds. Worries exist however that the SRM creates noice so it might not be the best choice for EVs. The Tesla Roadster uses an asynchronous machine, AM [27]. Both the SRM and the AM are very interesting due to high magnetic prices. The most commonly used machine is anyway the permanent magnet synchronous machine, PMSM. Since it is the most common choice it will be the one analyzed in this thesis. Electric machines used in EVs has to be able to produce enough torque at a large speed range. To maximize the use of the machine it is beneficial to use the machine in the constant power region as much as possible to minimize the size, see [28].

In order to calculate the losses in the inverter, the waveforms of the currents and voltages to the electric machine are needed. The electric machine used in this thesis is the one analyzed in [29] and [30]. It is a permanent magnet synchronous machine, PMSM, with a different inductance in the d and q direction. This gives the possibility to achieve a reluctance torque as well as a magnetic torque. The PMSM machine is modeled in steady state with the following equations when neglecting the magnetic losses.

$$u_{sd} = R_s i_{sd} - \omega_{el} L_q i_{sq} \tag{2.41}$$

$$u_{sq} = R_s i_{sq} + \omega_{el} L_d i_{sq} + \omega_{el} \psi_m \tag{2.42}$$

$$T_e = \frac{3}{2} p[\psi_m i_{sq} + (L_d - L_q) i_{sq} i_{sd}] \tag{2.43}$$

$$U_{phase_{RMS}} = \sqrt{\frac{u_{sd}^2 + u_{sq}^2}{2}} \tag{2.44}$$

$$I_{phase_{RMS}} = \sqrt{\frac{i_{sd}^2 + i_{sq}^2}{2}} \tag{2.45}$$

$$\varphi = \angle \vec{u_s} - \angle \vec{i_s} \tag{2.46}$$

The machine is controlled with MTPA (Maximum Torque Per Ampere) control and with a phase voltage limitation and a current limitation. When the voltage limit is reached, the machine is controlled with field weakening until the maximum current is reached according to the procedure described in [29]. The chosen current vector when using MTPA is seen in Fig. 2.12, the field weakening is however not shown in this figure.

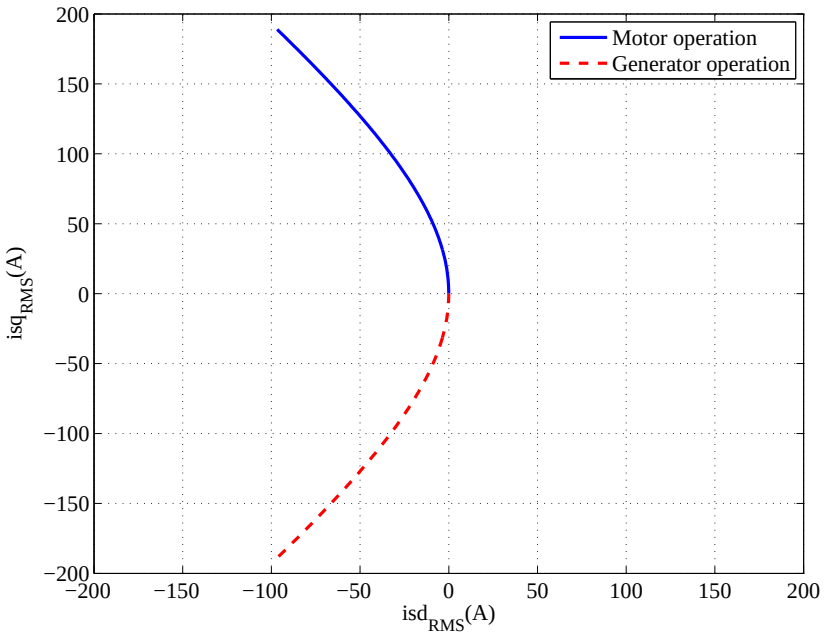

Figure 2.12: Resulting current vector when using MTPA, field weakening due to limited voltage is not shown

2.7 Charger

In [14] different topologies for on board chargers are discussed. An advantage with an on-bord charger is that the already existing propulsion inverter can be used as a charger. Some topologies even use the inductances in the electric machine as a filter component during charging operation. In [31] the demands for a charger for an electric vehicle is discussed. It is stated that the need for control of the power factor is needed, it is also important to make sure that the SOC distribution in the battery is constant during charging. Reference [32] states that the MLI has a power factor close to unity when rectifying AC to DC during charging operation. In [33] the infrastructure perspective of the charging of EVs are discussed. A need for bidirectional chargers is discussed. By being able to inject active power to the grid, the grid can be made stronger and more stable. Reference [34] and [35] propose a charger where the components of the already existing propulsion drive line is used. The results show that the performance of a charger made up by the already existing components is good. The same result is shown by [36] where different advantages of the different topologies are stated.

Using the inverter as a charger, as is done in this thesis, seems to be a beneficial choice from many perspectives.

2.8 BMS

In [37] studies are made of series connected H-bridges to achieve an even SOC distribution in the battery. The results show that with proper control the SOC distribution can be held constant. Reference [32] shows that both during charging as well as propulsion operation the MLI can act as a BMS and control which battery module that the energy is moved from/to.

2.9 Boundary conditions and load/charging cycles

2.9.1 Drive cycles

When analyzing energy consumption of vehicles, different drive cycles are used to compare vehicles. In this thesis, four different drive cycles are used, see Fig. 2.13 and Table 2.1. The driving cycles are used to determine the losses in both the battery and in the inverter to draw conclusions about the possibilities for a multilevel inverter in electric vehicles.

The first is the New European Driving Cycle, NEDC. The NEDC driving cycle is designed to represent the way vehicles are used in Europe and was introduced 1990. It is made up from four repetitions of the city driving cycle ECE15, and one high speed driving cycle, EUDC. The average speed of the vehicle is 33 km/h and the maximum speed is 120 km/h. The driving cycle has received much critic lately since it does not represent the way cars are used. Modern vehicles have much more power than 20 years ago and are driven with steeper accelerations.

The second drive cycle is the EPA Federal Test Procedure, FTP75. This drive cycle is used in the United states to specify the fuel consumption of an vehicle. This drive cycle has the same average speed as NEDC but the top speed is much lower, only 91 km/h. The driving cycle has also gotten criticism for being not aggressive enough and is therefore complimented with the US06, described more below.

The third drive cycle analyzed is the EPA Highway Fuel Economy Cycle, HWFET. This drive cycle aims at light duty trucks and is included in this thesis to show the behavior of the multilevel inverter for small trucks. The HWFET is a much less dynamic drive cycle than the ones for cars.

The last drive cycle is the US06 Supplemental Federal Test Procedure, US06. It is a very aggressive drive cycle compared to the others; the accelerations are harder and the top speed goes up to 129 km/h. It is used as a compliment to the FTP75 to show a more realistic way of the usage of the vehicle.

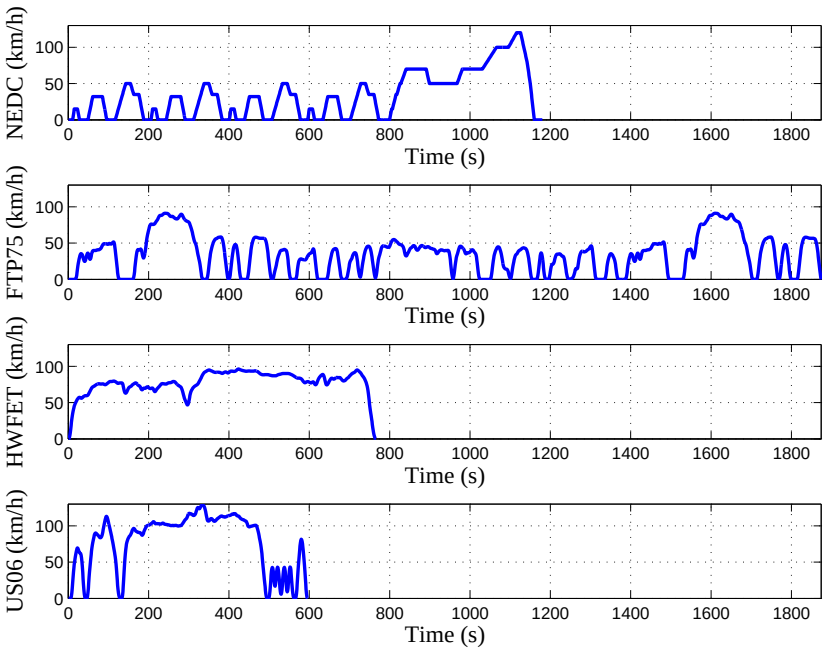

Figure 2.13: Speed profiles of the drive cycles

Table 2.1: Drive cycle parameters

Drive cycle	Speed avg [km/h]	Speed max [km/h]	Time [s]	Distance [km]	Energy regen [Wh/km]	Energy no regen [Wh/km]
NEDC	33	120	1180	10.9	54	82
FTP75	34	91	1874	17.8	44	80
HWFET	78	96	766	16.5	68	76
US06	78	129	596	12.9	83	117

2.9.2 Charging levels

To be able to have control over the current during charging, the voltage the inverter can produce needs to be higher than the grid voltage. In this thesis, the voltage the inverter can produce is designed to match the electric machine and is lower than the grid voltage, hence a transformer is needed. The transformer is modeled as an ideal transformer without losses, see Fig. 2.14. The losses in the transformer are neglected since it is assumed that the waveforms for both the MLI as well as the TLI are almost the same and therefore the losses will be approximately the same.

For the three phase charging, the transformer is assumed to supply the maximum voltage the inverter can produce, with a margin of 10 %.

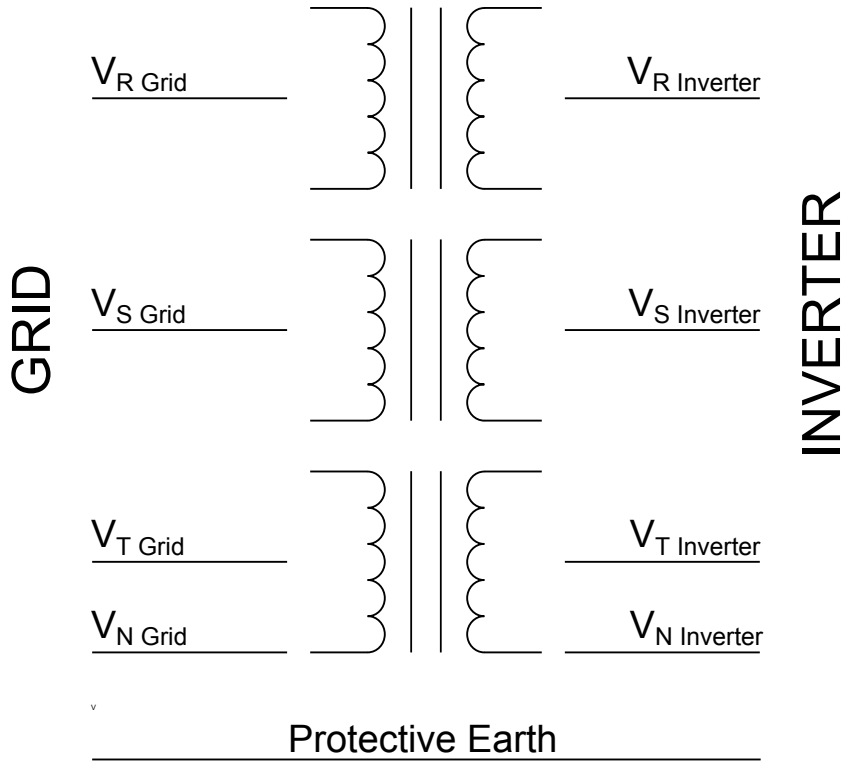

Figure 2.14: Charging transformer

Chapter 3

Case set-up and functionality verification

3.1 Case specification and parameter determination

3.1.1 Choice of DC-voltage

The motor analyzed in this thesis is designed for a phase voltage of maximum $106V_{rms}$. To be able to have control over the current, the voltage that the inverter can produce needs to be higher than the maximum voltage the motor needs. For the MLI, (2.16) describes the needed DC voltage to be able to produce 106 V with a margin of 10 % and is calculated to

$$V_{DC_{ML}} = \frac{U_{phase_{RMS\ MAX}}\sqrt{2}}{0.9 \cdot 1.07N} = 51V. \tag{3.1}$$

For the TLI the DC-voltage can be calculated using (2.12) and gives

$$V_{DC_{TL}} = \frac{U_{phase_{RMS\ MAX}}\sqrt{3}\sqrt{2}}{0.9} = 289V. \tag{3.2}$$

3.1.2 Component values

The electric machine used for the analysis in this thesis is a PMSM machine with parameters according to Tab. 3.1 and is referred to as the main machine. As a reference, a 10 pole machine will be used which has a lower magnetization. This one is referred to as the alternative machine.

The selected IGBT and diode combination for the TLI is chosen to SKIM909GD066HD and the MOSFET and diode combination for the MLI

Table 3.1: Parameters of the electric machine

Parameter	Main machine	Alternative machine	Unit
L_d	230	150	mH
L_q	500	300	mH
R_s	7.9	20	$m\Omega$
Pole pairs	2	5	
ψ_m	104	33	mWb
Maximum phase voltage	106	106	V_{RMS}
Maximum phase current	212	212	A_{RMS}
Maximum torque	112	109	Nm
Maximum power	66	49	kW

is chosen to IPB025N10N3, see Table 3.2. They are chosen to make the comparison fair since they have about the same relative margin to the breakdown voltage. To make the current rating equal, the MOSFETs will be placed with 5 in parallel.

Table 3.2: Parameters of power electronic components

Parameter	SKIM909GD066HD	IPB025N10N3	Unit
Nr in parallel	1	5	Pcs
Rated voltage	600	100	V
Rated current	900	180	A
$V_{t_{transistor}}$	0.7	0	V
$R_{on_{transistor}}$	2.1	2.0	$m\Omega$
T_{on}	271	58	ns
T_{off}	780	28	ns
$V_{t_{Diode}}$	1	Not in use	V
$R_{on_{Diode}}$	0.94	Not in use	$m\Omega$
K_{rr}	86	43	$nJV^{-1}I^{-1}$

The vehicle analyzed is a small compact car with the data given in Table 3.3.

Table 3.3: Car parameters

Parameter	Value	Unit
Weight	1100	kg
$A \cdot C_d$	0.45	Nv^{-2}
Friction coefficient	0.01	N
Wheel radius	0.33	m
Gearbox ratio	11.5	
Gearbox efficiency	90	%

The battery cells are assumed to have a resistance of 2 $m\Omega$ with a nominal voltage of 3.7 V and an energy content of 92.5 Wh. The battery for both the TLI drive system and the MLI drive system consist of 108 of these cells building up a capacity of 10 kWh.

3.1.3 Machine operation points

Operating the electrical machine at different torques and speeds gives the operation points according to Fig. 3.1, Fig. 3.3 and Fig. 3.5 for the main machine. In the figures, the operation points of the NEDC driving cycle is also given as a reference of where the electric machine is typically used. In Fig. 3.3 it can be seen that the voltage increases with speed up to the field weakening region. When the maximum voltage is reached the machine can continue to increase its speed by demagnetising the machine. This is done by increasing the current in the d-direction giving an increased current without increasing the torque. This can be seen in Fig. 3.1 where the straight current lines bends down when entering the field weakening region. Its also observable in Fig. 3.5 that the current leads the voltage in the field weakening region due to that we need to use a current to demagnetize the machine.

The operating points for the alternative machine is shown in Fig. 3.2, Fig. 3.4 and Fig. 3.6. It can be seen that the power factor is worse for low speed operation but for high speed operation the power factor becomes much better.

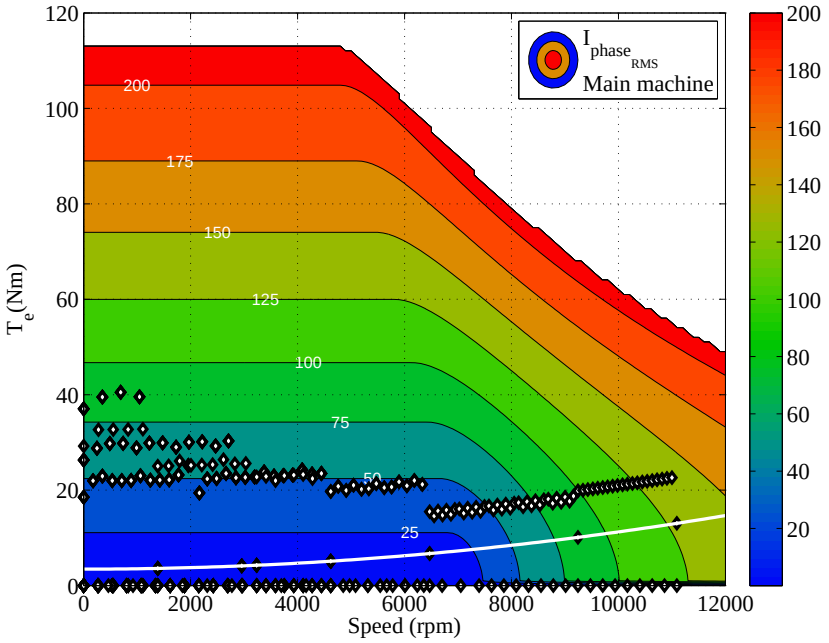

Figure 3.1: RMS-value of the phase currents when using the main machine. The NEDC driving cycle is marked for reference. The white line shows the torque needed to propel the vehicle at constant speed.

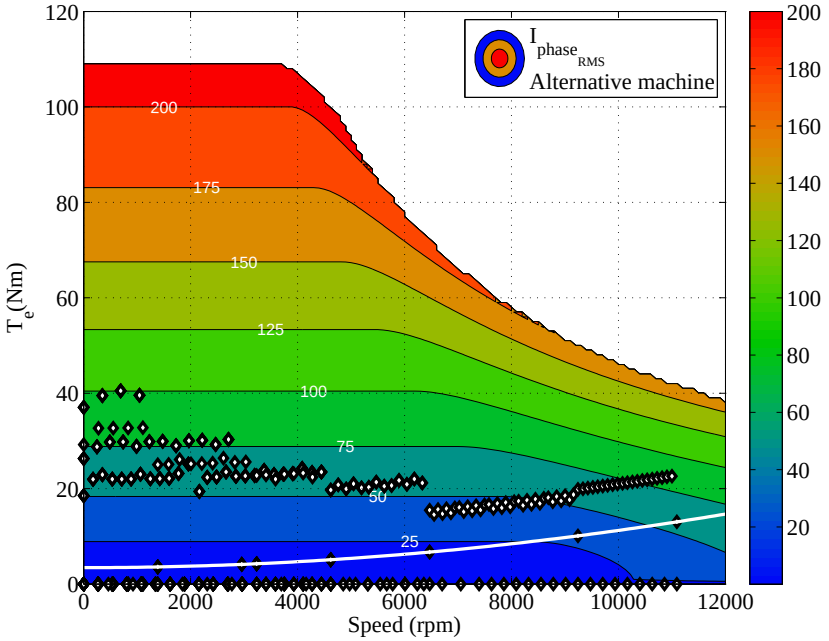

Figure 3.2: RMS-value of the phase currents when using the alternative machine. Description as in Fig. 3.1

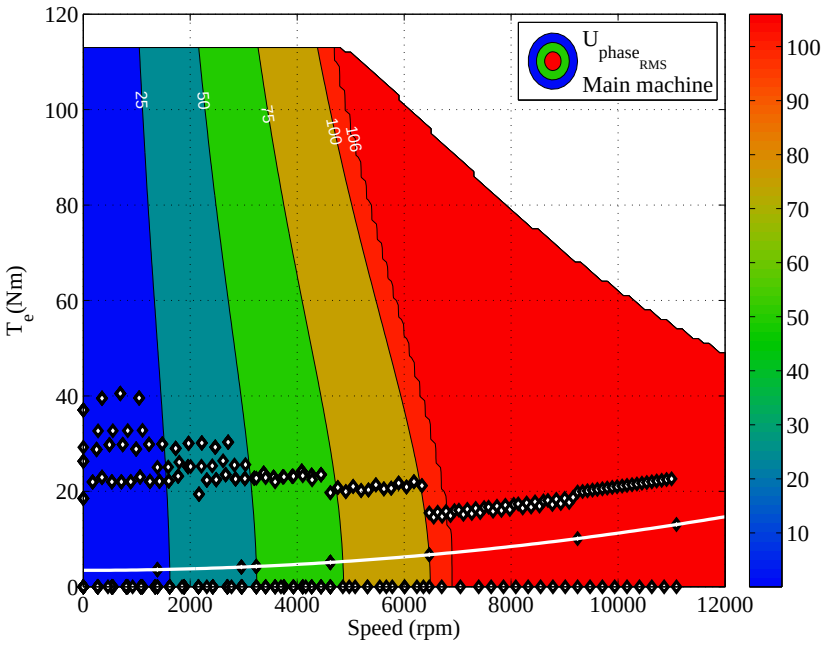

Figure 3.3: RMS-value of phase voltages when using the main machine. Description as in Fig. 3.1

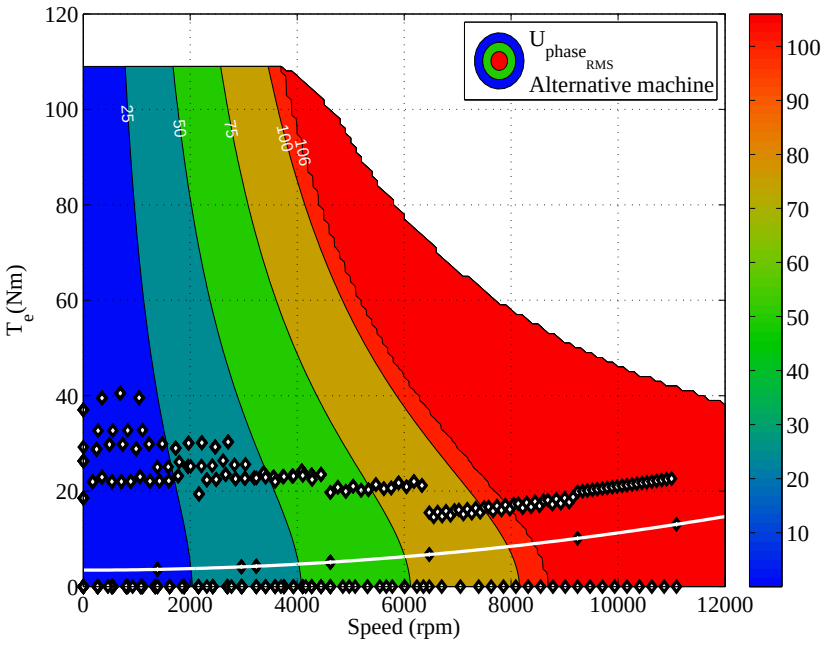

Figure 3.4: RMS-value of phase voltages when using the alternative machine. Description as in Fig. 3.1

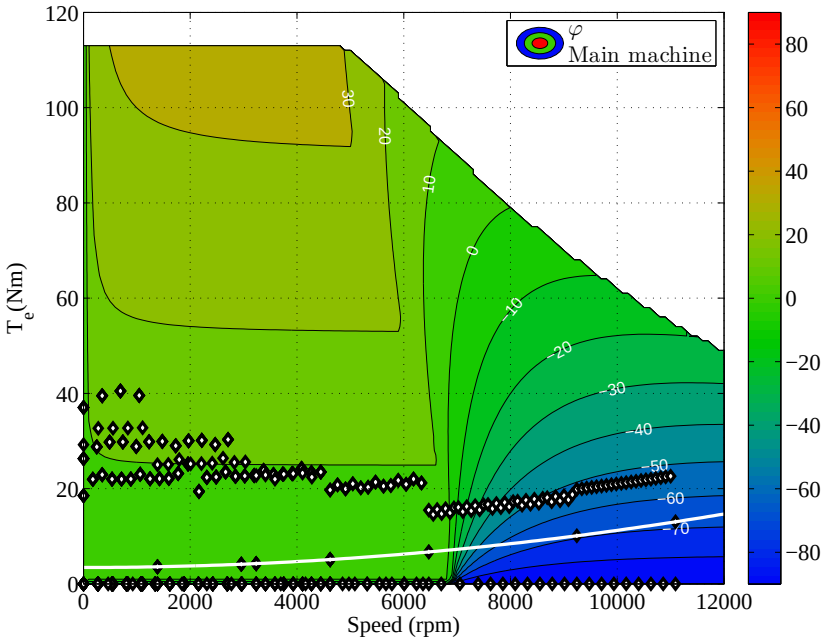

Figure 3.5: Phase difference between voltage and current when using the main machine. Description as in Fig. 3.1

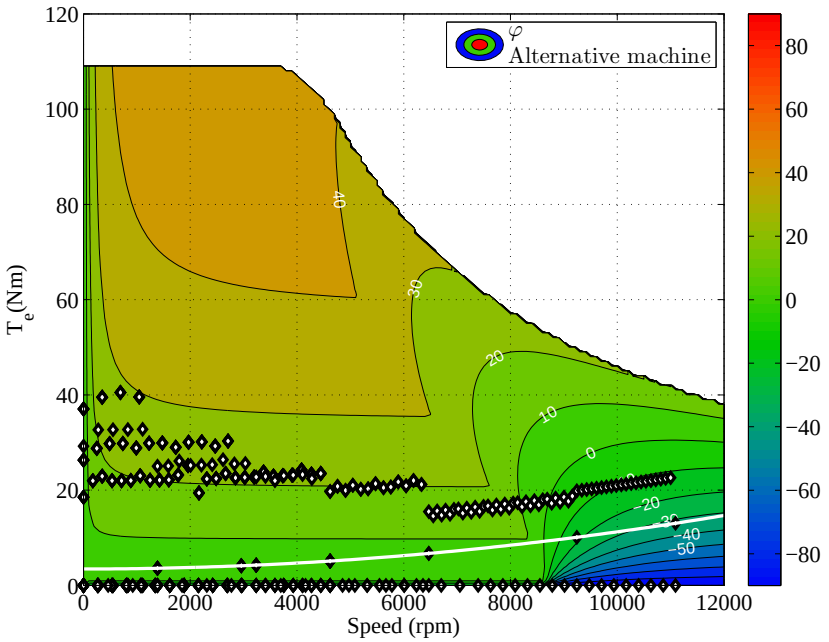

Figure 3.6: Phase difference between voltage and current when using the alternative machine. Description as in Fig. 3.1

3.2 Experimental setup

To verify the waveforms created by the MLI an experimental setup is designed. The inverter will be used to verify the wave shapes used in the analytical analysis. The experimental MLI can be seen in Fig. 3.7. In the MLI the MOSFET IRF1324S-7PPbF is used. The on resistance ($R_{on_{MOSFET}}$) of this MOSFET is only maximum 1 $m\Omega$. The voltage capabilities for this MOSFET is only 24 V so it is only used to verify the capability to produce the waveforms analysed.

Figure 3.7: Laboratory setup of the 7-level multilevel inverter. The 3 phases consist of 3 levels each. The battery inputs are shown in the lower part of the picture, the outputs are on the left side of the groups and the common Y-connection point is shown on the right sides of the groups

Chapter 4

Experimental results

4.1 Output waveforms and harmonics

Fig. 4.1, 4.2 and 4.3 show the output voltage from the MLI at $m_a = 0.5$, $m_a = 1.0$ and $m_a = 1.2$. It can be seen that the first harmonic in the line to line voltage is no 11 for $m_a = 0.5$ and $m_a = 1.0$. When operating at $m_a = 1.2$ the possibility to eliminate harmonic 5 and 7 is removed. In Fig. 4.4 and 4.5 the 5th and the 7th harmonic are plotted for different m_a. It shows a good match with the analytical calculations in Fig. 2.7.

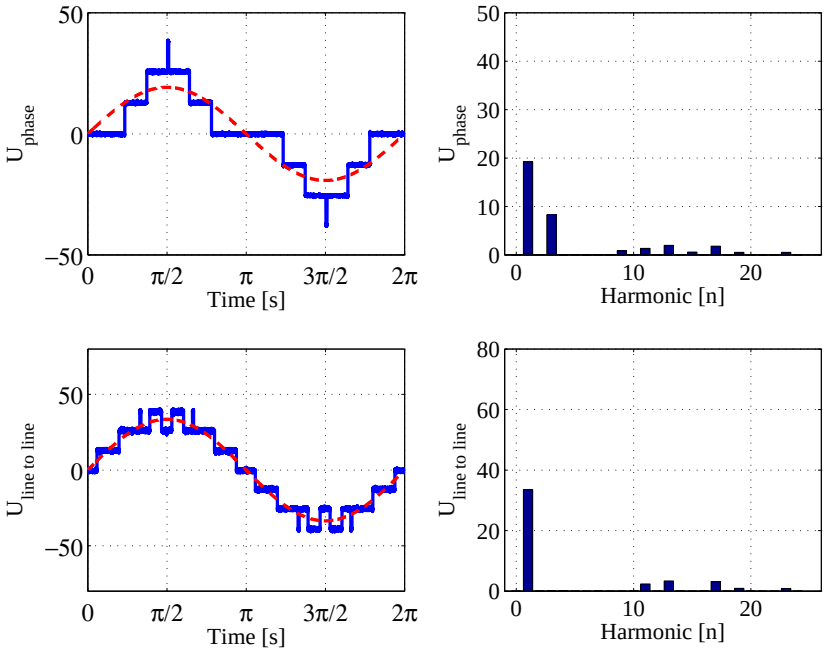

Figure 4.1: Measured voltage output and harmonic content at $m_a = 0.5$

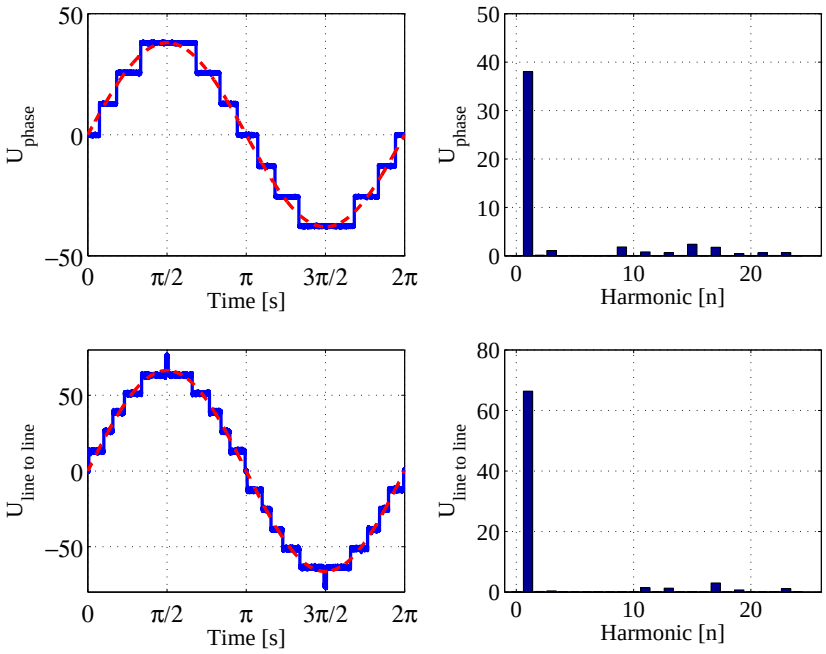

Figure 4.2: Measured voltage output and harmonic content at $m_a = 1.0$

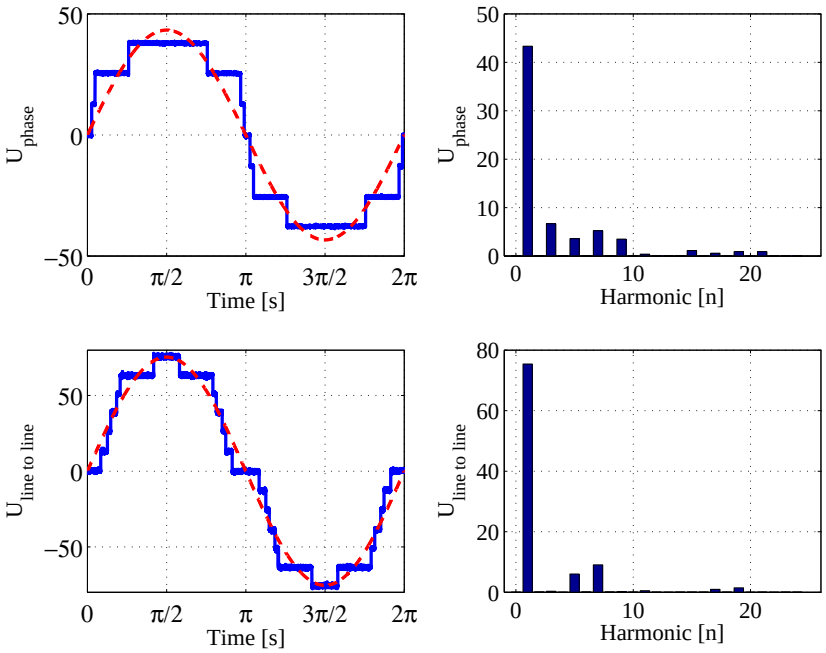

Figure 4.3: Measured voltage output and harmonic content at $m_a = 1.2$

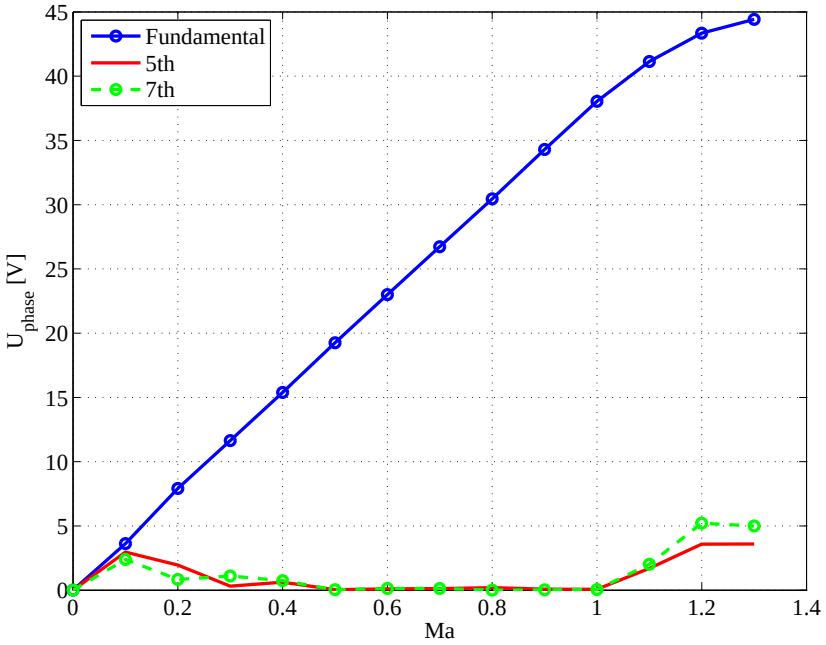

Figure 4.4: Measured fundamental, 5th and 7th harmonic in the phase voltage

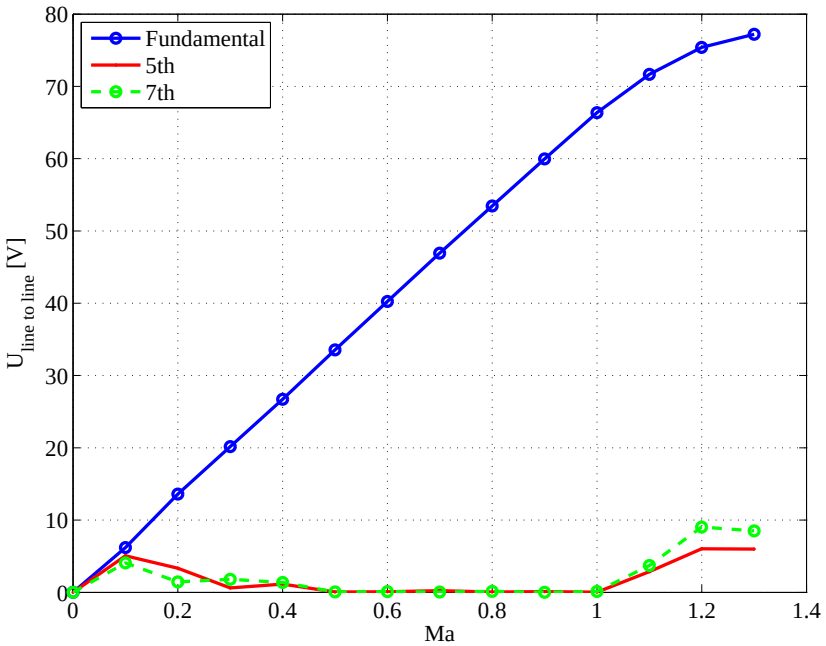

Figure 4.5: Measured fundamental, 5th and 7th harmonic in the line to line voltage

4.2 Total Harmonic Distortion

The total harmonic distortion, THD, for the output voltage is both simulated and measured for different magnitudes of the output voltage. The THD is calculated with help of the RMS value and its definition range is therefore very high. The simulations and the measurements can be seen in Fig. 4.6 and shows a good match. The current THD is not calculated or measured since it is a function of the output frequency as well as the machine operating point.

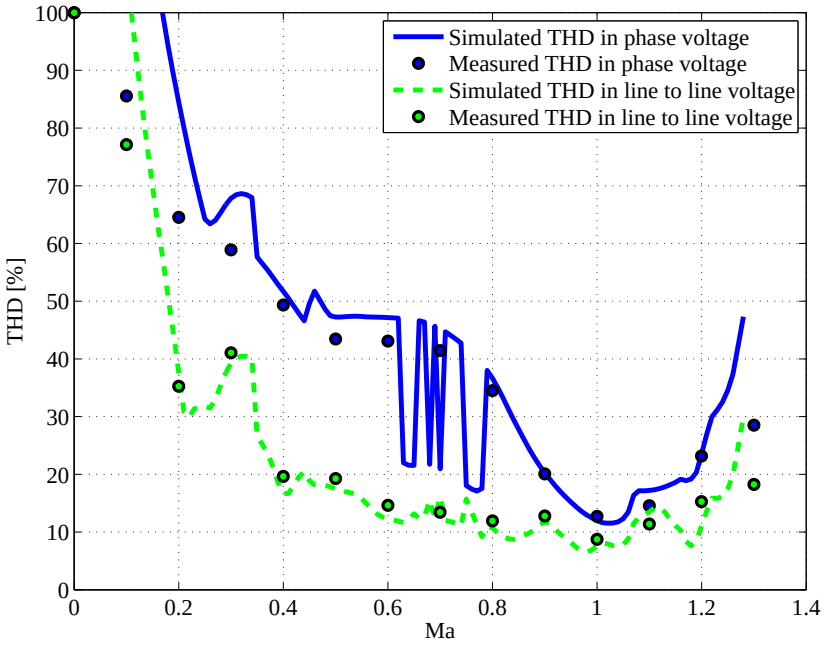

Figure 4.6: Simulated and measured voltage THD for the MLI

It can be seen that the THD is as lowest at $m_a = 1$, then the THD is down to under 10 % for the line to line voltage.

4.3 Balancing

The possibility to balance the battery cells is evaluated with the MLI test setup. The energy sources is chosen to small super capacitors with a capacitance of 10 F each. The three capacitors in one leg are charge to 1.6 V, 1.8 V and 2.3 V. The inverter is then operated at $m_a = 1$ to a resistive load to to verify that the inverter will balance the cells during sine wave operation. The control strategy is to use the inverter with the highest voltage as the inverter controlled with α_1, and the inverter with the lowest voltage as the one controlled with α_3.

In Fig. 4.7 the super capacitor voltages are plotted over time, it can been seen that the capacitors will have the same voltage after some time. Since the A/D-converter for this setup has a very poor resolution, the cells does not get perfectly balanced. When the control system measures that the cells are equal, balanced, it always uses the first H-bridge (green curve) as the one controlled with α_1, the second (red curve) with α_2 and the third (blue curve) with α_3. This unfortunately causes the cells to never be totally balanced in this setup, they will be unbalanced with the resolution of the A/D-converter.

Interesting to notice is that if m_a would have been lower, the balancing would be even more efficient since the lowest cell would never be connected to the load.

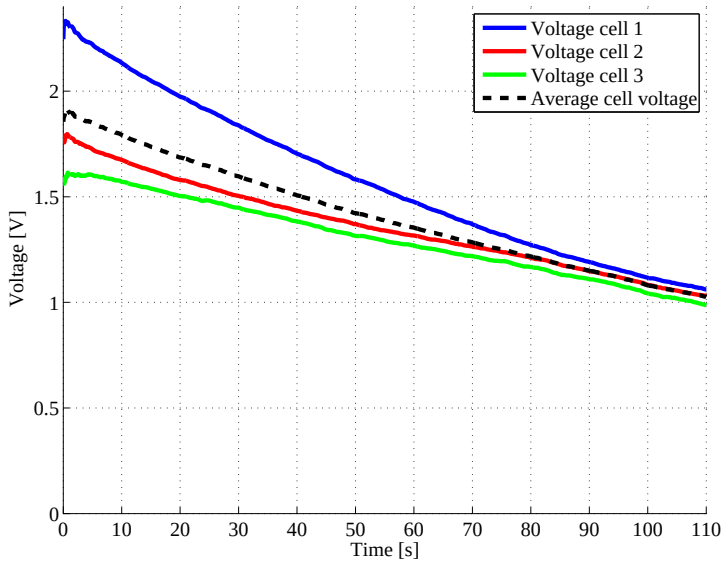

Figure 4.7: Measured balancing performance. The three cell voltages in one leg converges to the same voltage level over time when operating the MLI as a propulsion inverter or a charger

4.4 Battery current

In Fig. 4.8 the inverter is operated at $m_a = 1$ and $f_{fundamental} = 50\ Hz$. The load consists of an RL load with $R = 11\ \Omega$ and $L = 36\ mH$. The current in the battery groups can be seen in Fig. 4.9, 4.10 and 4.11. They match the theoretical analysis seen in Fig. 2.8, 2.9 and 2.10.

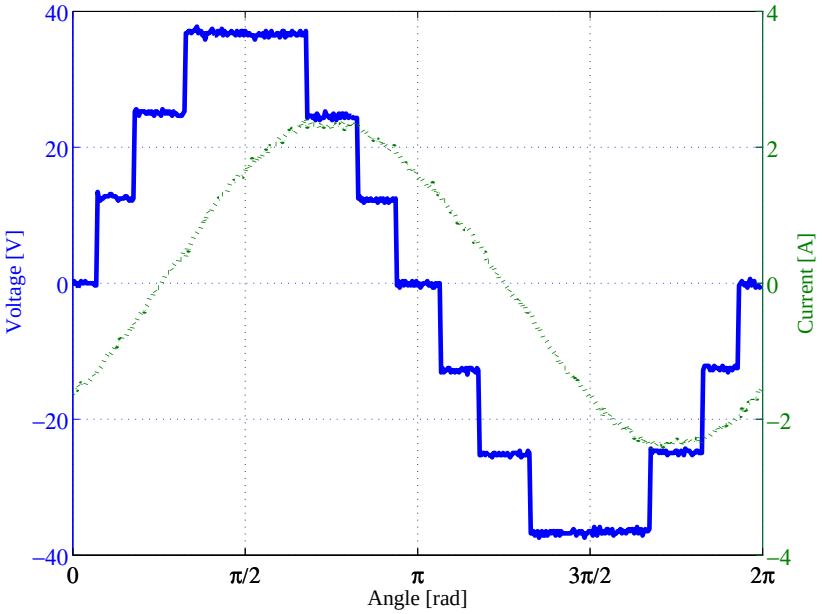

Figure 4.8: Measured output phase voltage and current

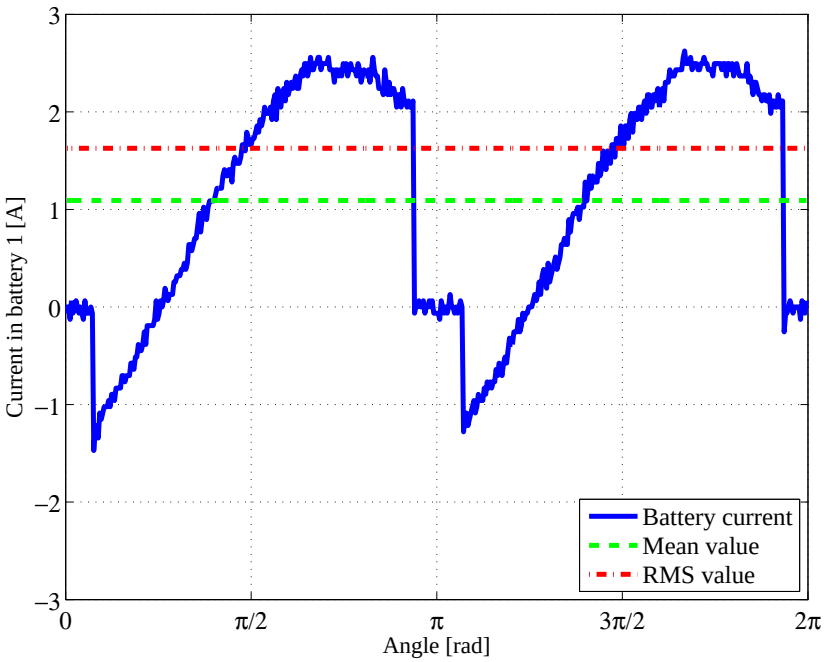

Figure 4.9: Measured current in battery group 1

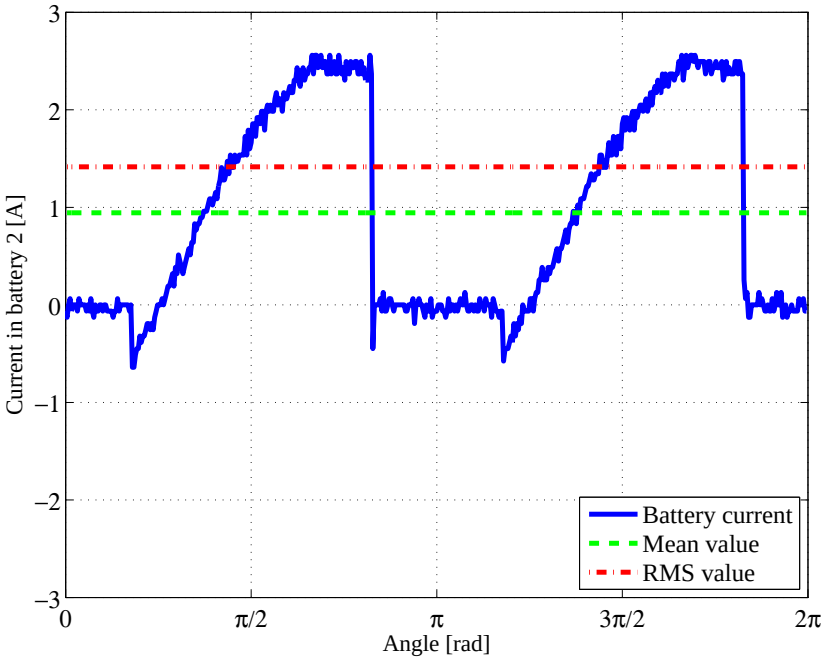

Figure 4.10: Measured current in battery group 2

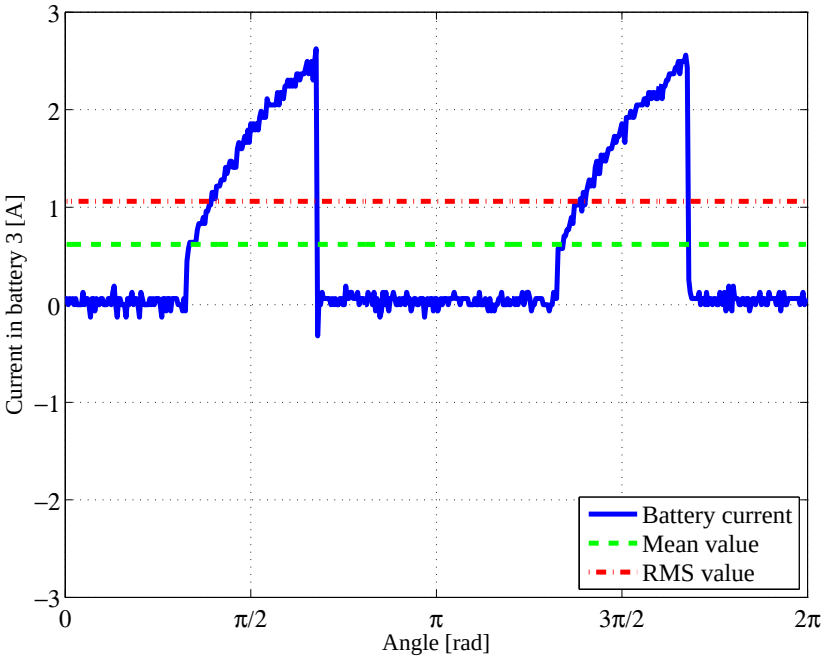

Figure 4.11: Measured current in battery group 3

Chapter 5

Static loss evaluation

5.1 Efficiency calculations

When an inverter is used to supply the electric machine in an electric vehicle, the losses are a function of the operation points of the car. Based on the operation points given in Fig. 3.1, Fig. 3.3 and Fig. 3.5 the losses in the inverter and in the battery are calculated.

5.1.1 Inverter

The losses in the two different inverters are calculated assuming that the current to the electrical machine is equal for the two cases and does not contain any harmonics.

Two level inverter

The power loss for the TLI using IGBTs is calculated for different torques and speeds and is shown in Fig. 5.1 for a switching frequency of 10 kHz. It can be seen that the losses increase quite proportionally to the current and so does also torque. The losses are not speed dependent until we reach the field weakening region and need a current to demagnetize the machine.

The efficiency of the inverter is shown in Fig. 5.2. Since the losses and the output power both increase proportionally to the torque, the efficiency of the inverter is not dependant of the torque. Since the losses are not dependant on the speed but the output power is, it can be seen that the efficiency increases with speed. At high speeds and low torques the output power is very low, but the inverter has a relatively high losses. These losses are due to that the inverter needs to supply a current to demagnetise the machine in the

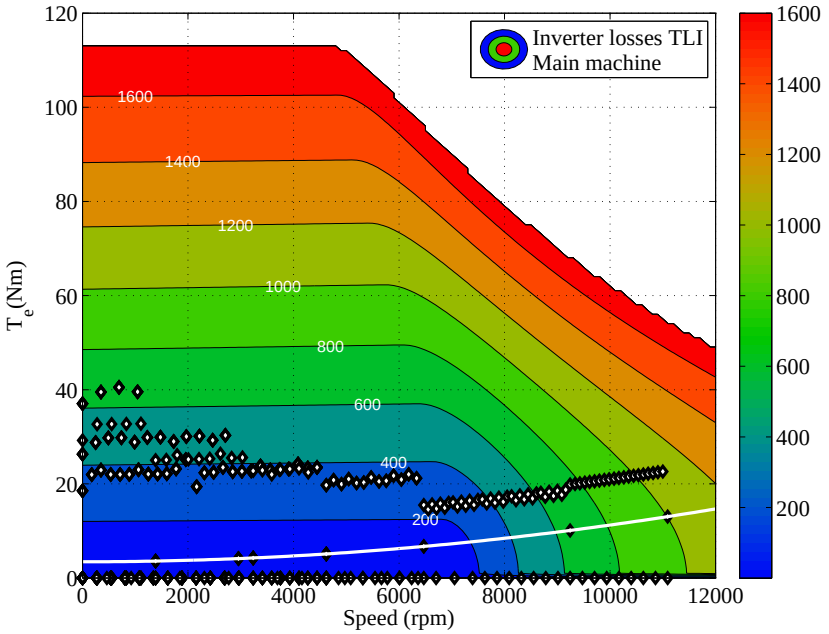

Figure 5.1: Inverter power loss for the TLI. Description as in Fig. 3.1

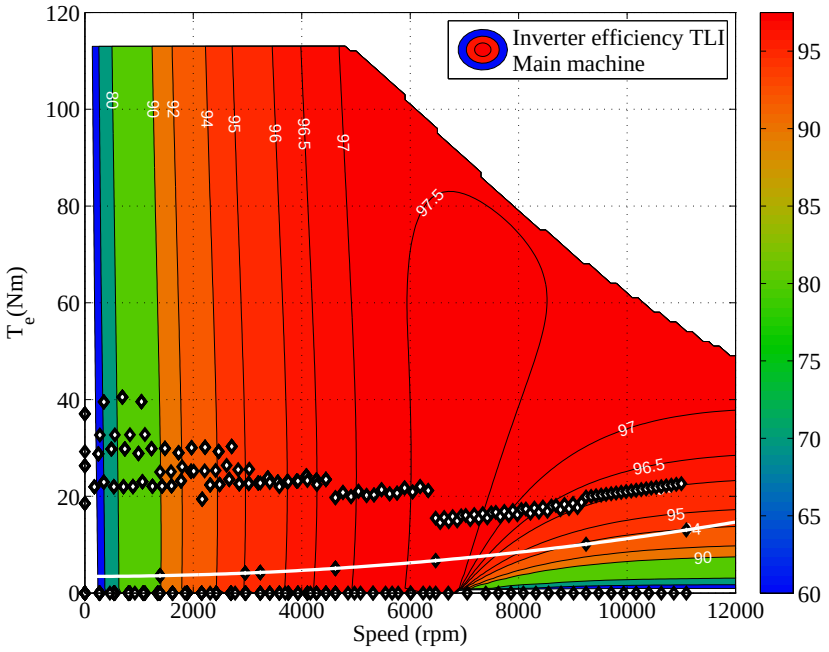

Figure 5.2: Inverter efficiency for the TLI. Description as in Fig. 3.1

field weakening region, and the inverter efficiency therefore drops at at high speeds.

Multilevel inverter

The inverter losses with the MLI at different speeds and torques produced by the electrical machine can be seen in Fig. 5.3. The conductive losses in the MOSFETs dominates the losses since the inverter is only switched at the fundamental frequency, even at the maximum speed, the switching losses never exceeds 20 W for the inverter. Since the conductive losses in a MOSFET is proportional to the square of the current, the losses increases with the square of the torque in the region without field weakening. In the field weakening region the losses increases for a certain torque, since all the extra current is needed to demagnetize the machine.

The efficiency of the MLI can be seen in Fig. 5.4. Since the power loss is proportional to the square of the torque and the output power is proportional to the torque, this means that at a certain speed the efficiency drops for higher torques. When increasing the speed, the output power increases and the losses remains fairly constant for a certain torque. This causes the efficiency to increase at higher speeds. When entering the field weakening region the efficiency drops since more current is needed to demagnetize the machine.

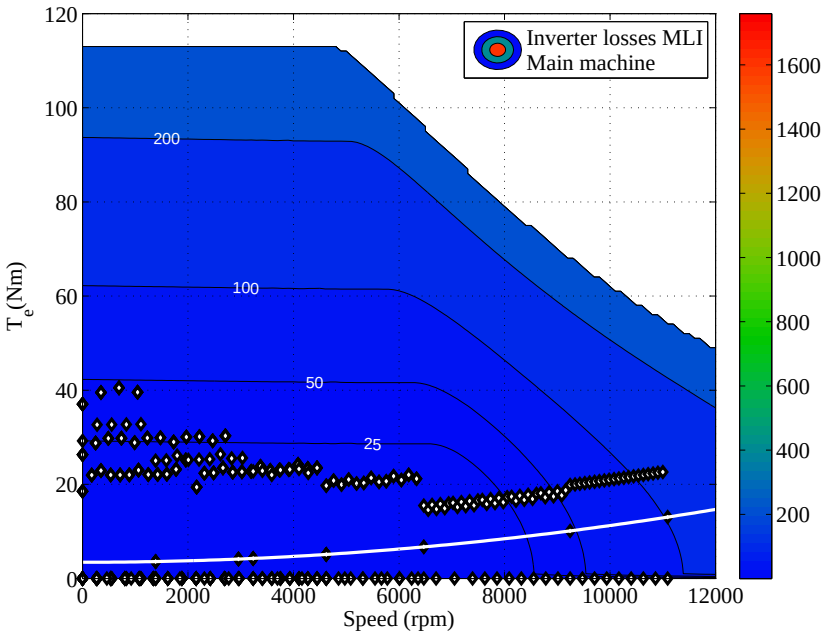

Figure 5.3: Inverter power loss for the MLI. Description as in Fig. 3.1

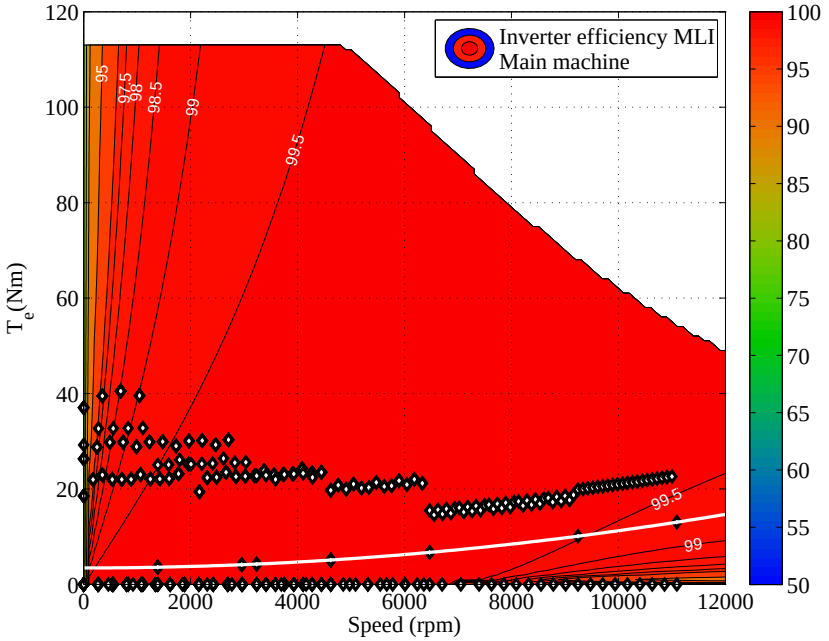

Figure 5.4: Inverter efficiency for the MLI. Description as in Fig. 3.1

5.1.2 Battery

The battery loss for the car when using a TLI is shown in Fig. 5.5. Since the whole battery supplies the power to the electric machine and the voltage in the battery is assumed to be constant, the battery current becomes proportional to the active power supplied to the machine. The losses in the battery then become proportional to the square of the electric machine power. This can be seen in Fig. 5.5 for all operation points. Due to that the TLI balances the reactive power in the separate phases already in the inverter and also smoothens a very high frequency ripple with its DC-link capacitor, the battery utilization becomes as good as it can be with the TLI. When switching to a MLI the question is, how much extra losses will be added.

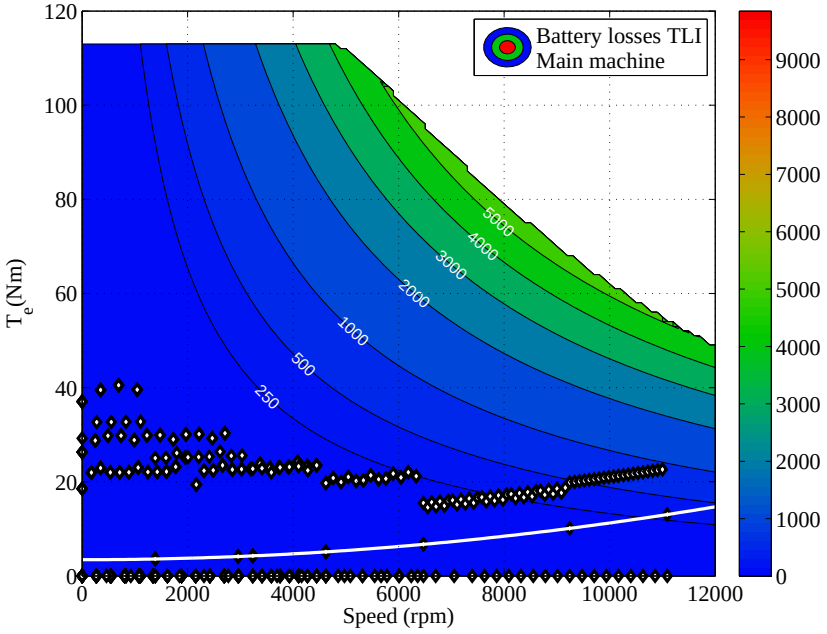

Figure 5.5: Losses in the battery when using a TLI. Description as in Fig. 3.1

The battery losses when operating the vehicle with infinity large capacitors to the input of a MLI can be seen in Fig. 5.6. The battery losses will be higher when using a MLI drive system compared to a TLI, even with these capacitors. This is due to that the current in the different groups will not be equal when operating the inverter with FSHE, even though the current will be pure DC.

The battery loss when operating the vehicle with a MLI without filter capacitors on the input of the H-bridges can be seen in Fig. 5.7. One can

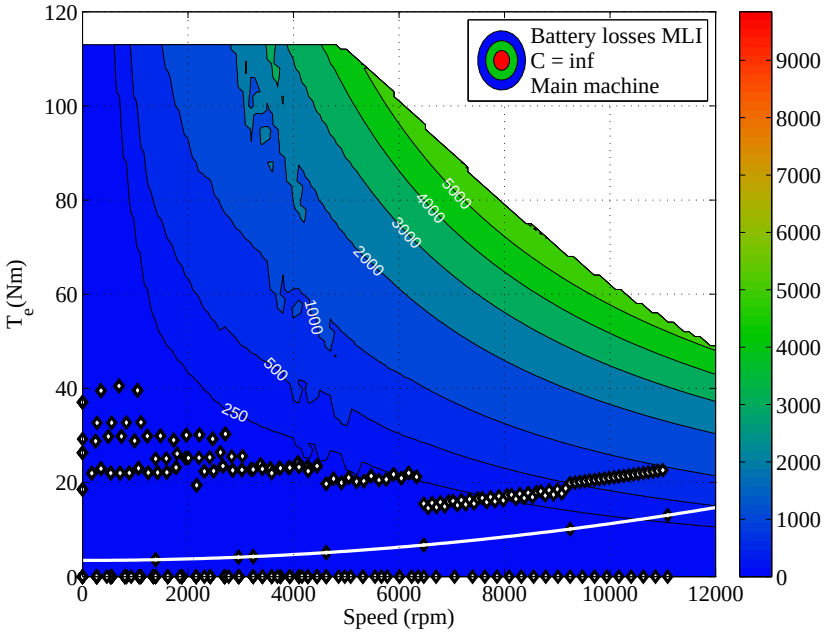

Figure 5.6: Losses in the battery when using a MLI with infinity large filter capacitances. Description as in Fig. 3.1

see that the losses are much higher now, the battery now needs to supply the reactive power but also take care of that the battery power is not taken out as a smooth current.

When using an input capacitor of 3.6 mF connected to each input, the losses can be seen in Fig. 5.8. Using these capacitors, the current out of the battery will be smoothen. The faster the machine runs, the higher the battery current frequency will be and therefore the battery loss reduction will be more favourable at high speeds.

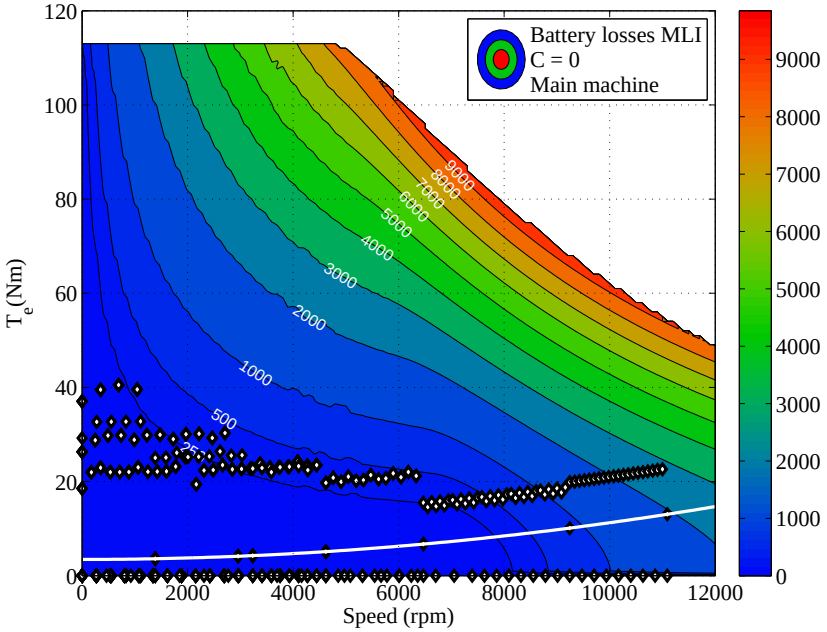

Figure 5.7: Losses in the battery when using a MLI without filter capacitances. Description as in Fig. 3.1

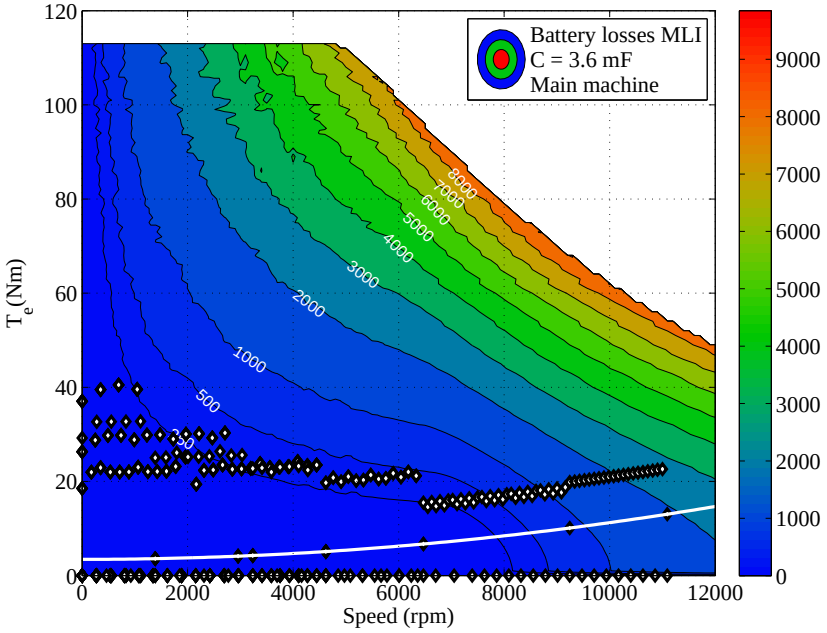

Figure 5.8: Losses in the battery when using a MLI with filter capacitances of 3.6 mF. Description as in Fig. 3.1

5.1.3 Total losses

The total losses that are analysed and that are presented below, consists of the inverter losses and the battery losses. The machine losses are assumed to be equal for the two inverters and are therefore excluded in this analysis.

For the TLI, the total losses of the battery and the inverter are shown in Fig. 5.9.

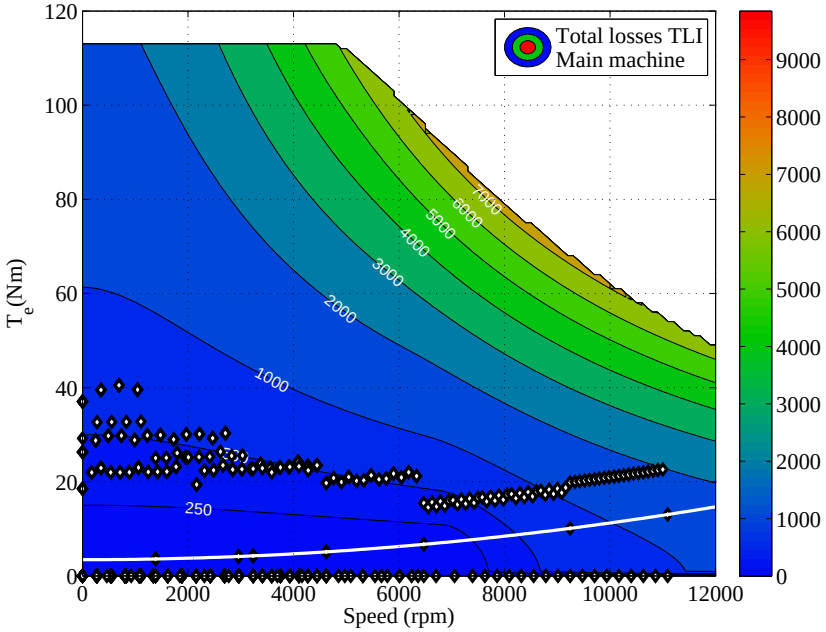

Figure 5.9: Inverter and battery losses for the TLI. Description as in Fig. 3.1

For the MLI with large capacitors in parallel to the input of the H-bridges, the losses are shown in Fig. 5.10, and for the MLI without input capacitors the losses are shown in Fig. 5.11. If the capacitors are chosen to 3.6 mF the losses can be seen in Fig. 5.12. The drive system with the MLI with capacitors shows an advantage over the TLI drive system at all operating points. For the MLI system without capacitors, as expected, the losses becomes larger than for the TLI systems for high speeds and torques.

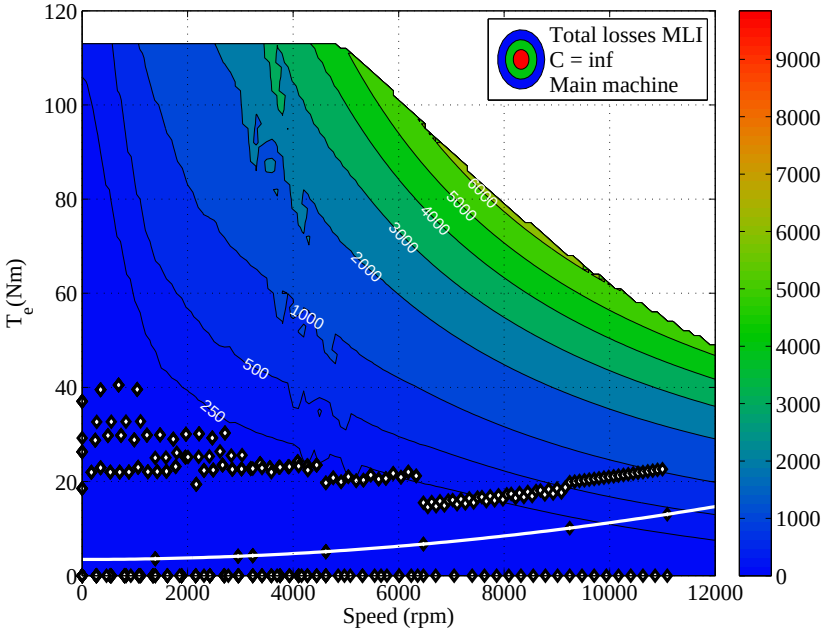

Figure 5.10: Inverter and battery losses for the MLI with capacitors. Description as in Fig. 3.1

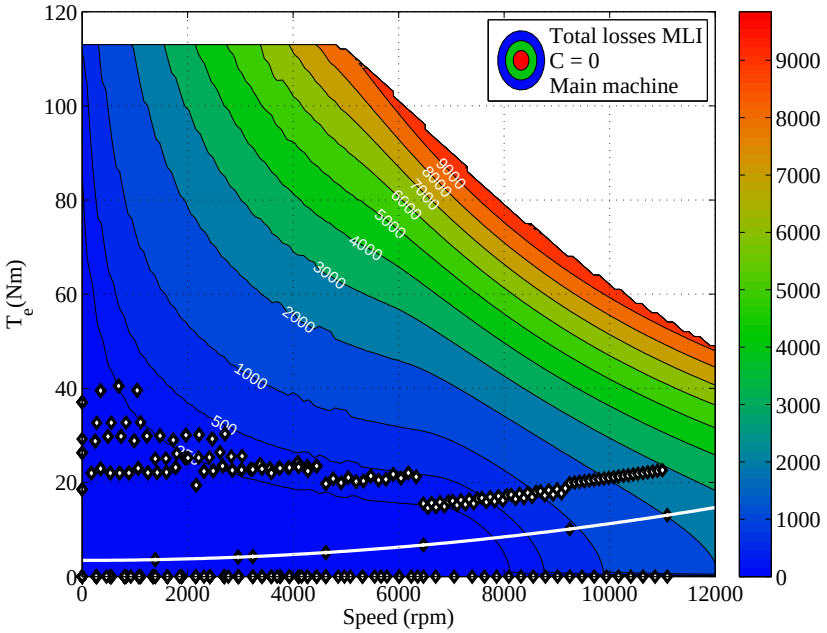

Figure 5.11: Inverter and battery losses for the MLI without capacitors. Description as in Fig. 3.1

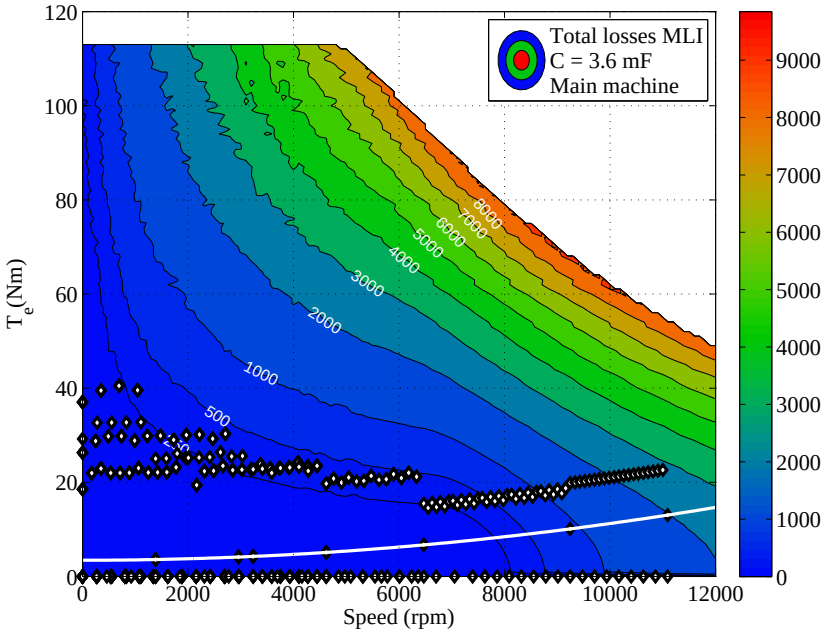

Figure 5.12: Inverter and battery losses for the MLI with filter capacitances of 3.6 mF. Description as in Fig. 3.1

5.1.4 Comparison

The losses in the inverters for different speeds and a fixed torque of 10 Nm are shown in Fig. 5.13, and for a torque of 60 Nm in Fig. 5.14. It can be seen that the MLI has lower inverter losses for all operating points. It can also be noticed that the inverter losses for both inverters increases a lot when entering the field weakening region.

The losses in the battery for different speeds and a fixed torque of 10 Nm are shown in Fig. 5.15, and for a torque of 60 Nm in Fig. 5.16. The losses in the battery for the TLI are lowest for all speeds. This is due to that the current out from the battery is pure DC. The battery losses for the MLI with infinity large capacitors to the inputs of the H-bridges are a bit higher. The batteries do not supply the reactive power but some of the battery modules have a higher current than other ones, even though they have a pure DC current. The losses for the MLI without capacitors are higher for all speeds, especially when entering the field weakening region. The batteries must then supply the reactive power needed by the electrical machine. When using an input capacitor of 3.6 mF the battery losses are reduced a bit compared to not having capacitors, this is most obvious for higher torques.

The total losses for the drive systems for different speeds and a fixed torque of 10 Nm is shown in 5.17, and in Fig. 5.18 the total losses are shown for a torque of 60 Nm. When operating the machine at low torques, the losses for the MLI drive system are lower for low speeds. When entering the field weakening region the battery losses increase drastically for the MLI drive system if the reactive power can not be supplied from the capacitors instead of the battery. For higher torques the TLI drive system shows lower losses for almost all speeds, if one does not have the possibility to filter out the reactive power and the harmonic content from the battery in the MLI drive system. The electric machine will on the other hand not operate at this high torque very often, as will be showed later on.

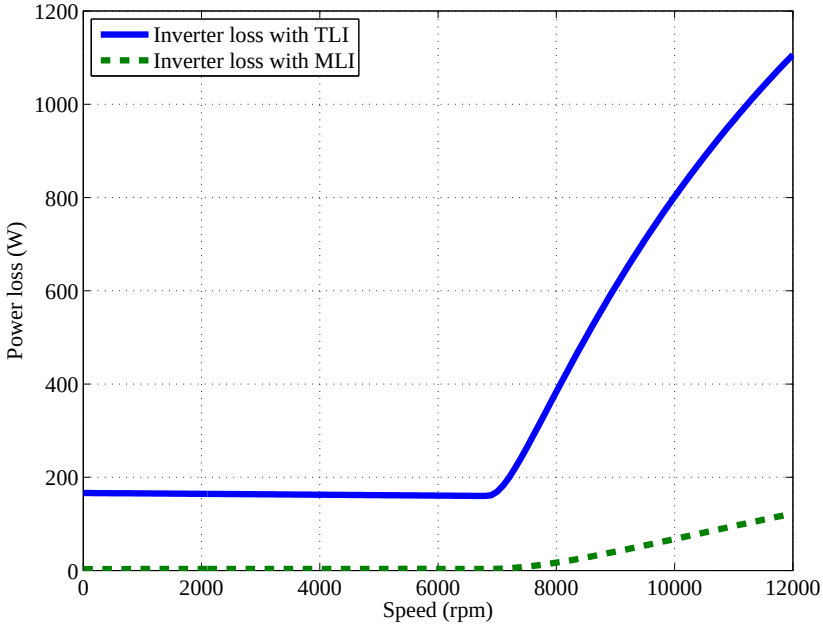

Figure 5.13: Inverter power loss for T=10 Nm

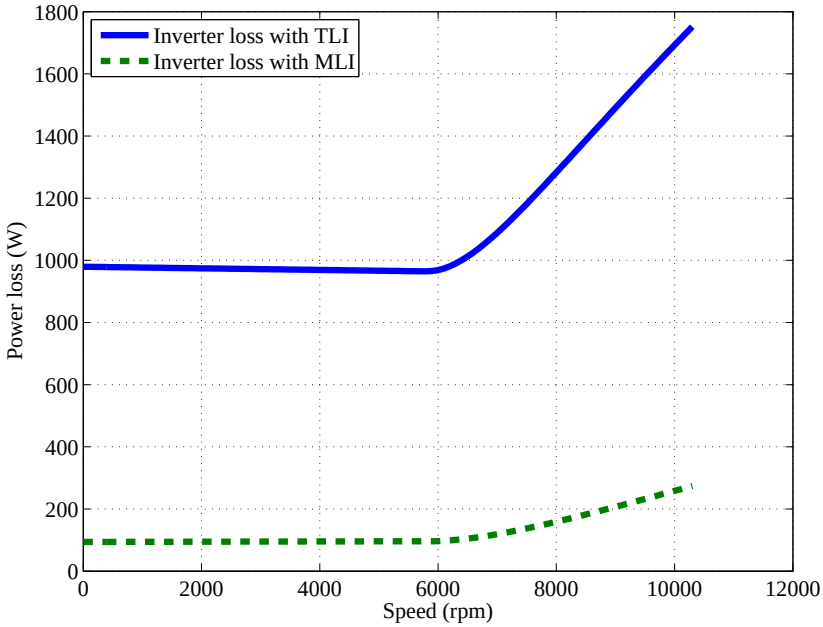

Figure 5.14: Inverter power loss for T=60 Nm

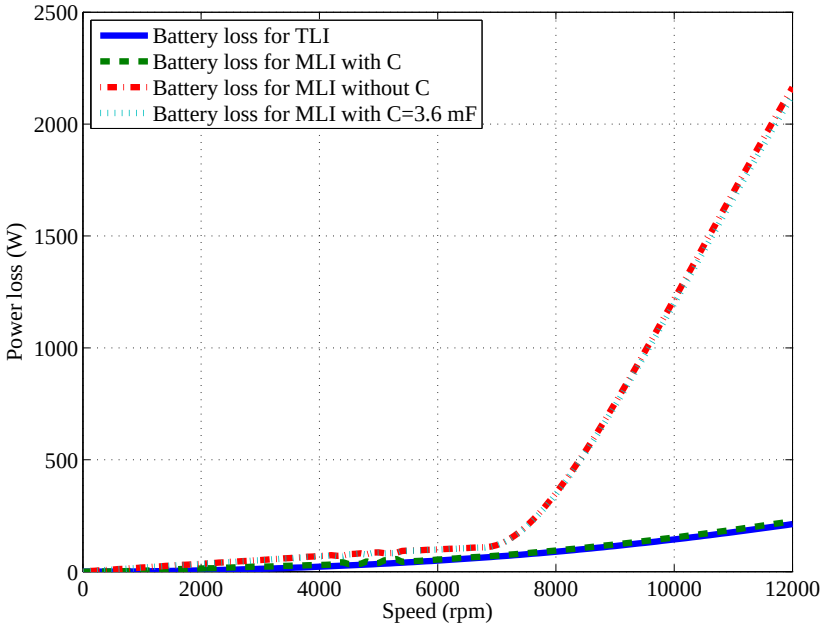

Figure 5.15: Battery power loss for T=10 Nm

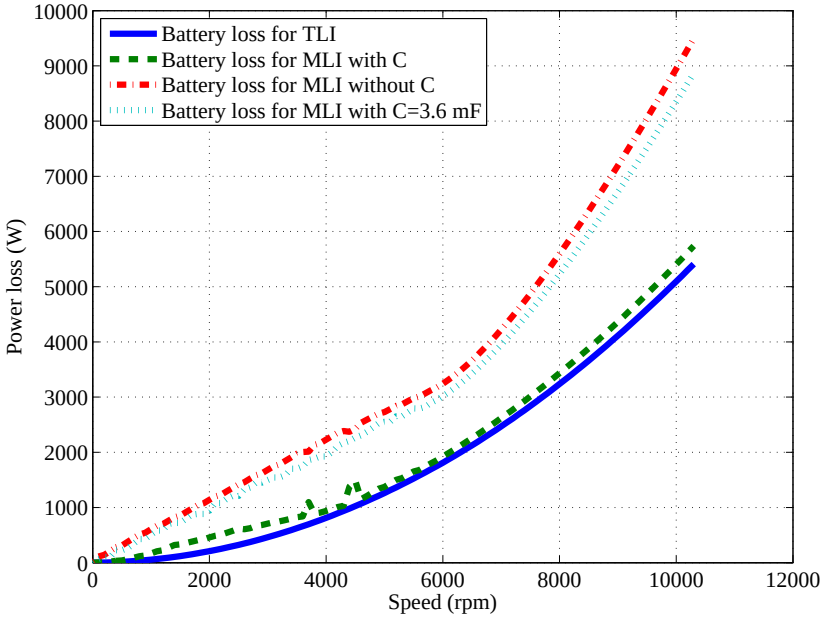

Figure 5.16: Battery power loss for T=60 Nm

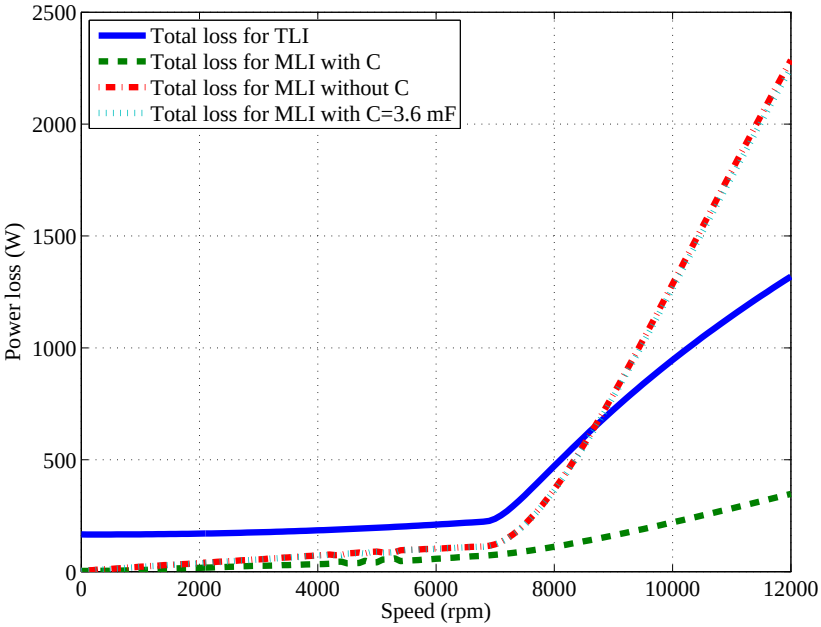

Figure 5.17: Total loss for T=10 Nm

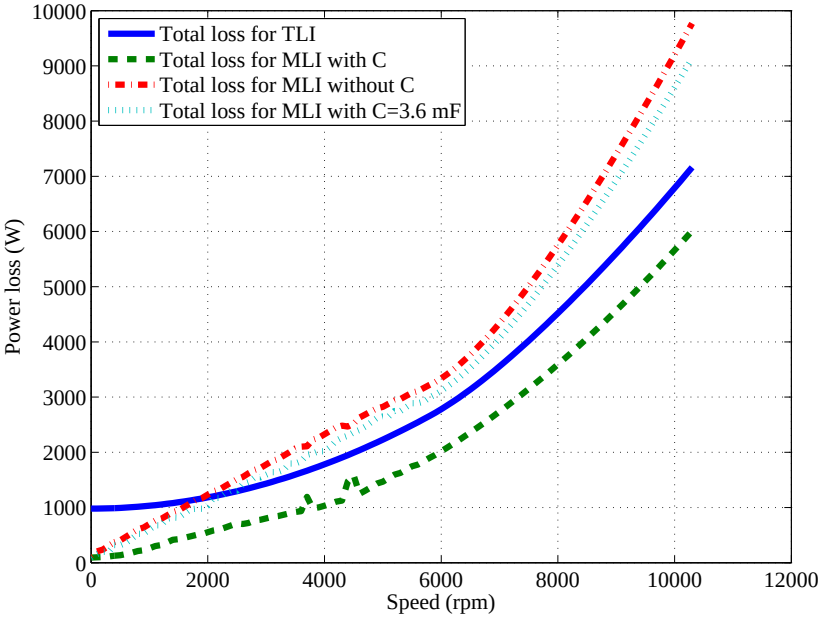

Figure 5.18: Total loss for T=60 Nm

5.1.5 Charging

The losses when using the inverter as a charger can be seen in Fig 5.19 and in Table 5.1. For the two lower power alternatives the MLI shows a benefit in efficiency, for higher power the battery losses increase compared to the TLI case if the battery current is not filtered. The efficiency is shown in Fig. 5.20. It is seen that the efficiency is higher at the lowers input current and that the MLI is the most attractive alternative, especially if the possibility to filter the battery current exists. The efficiency during charging might on the other hand not be such an important design criteria, it is more important to be able to control where the losses occur.

Table 5.1: Total losses for different charging power

Charging	Input Power	TLI	MLI $C = \infty$	MLI $C = 0\ mF$	MLI $C = 3.6\ mF$
3 Phase 10 A	6900 W	225 W	66 W	105 W	103 W
3 Phase 16 A	11040 W	419 W	169 W	268 W	264 W
3 Phase 32 A	22080 W	1150 W	676 W	1072 W	1058 W

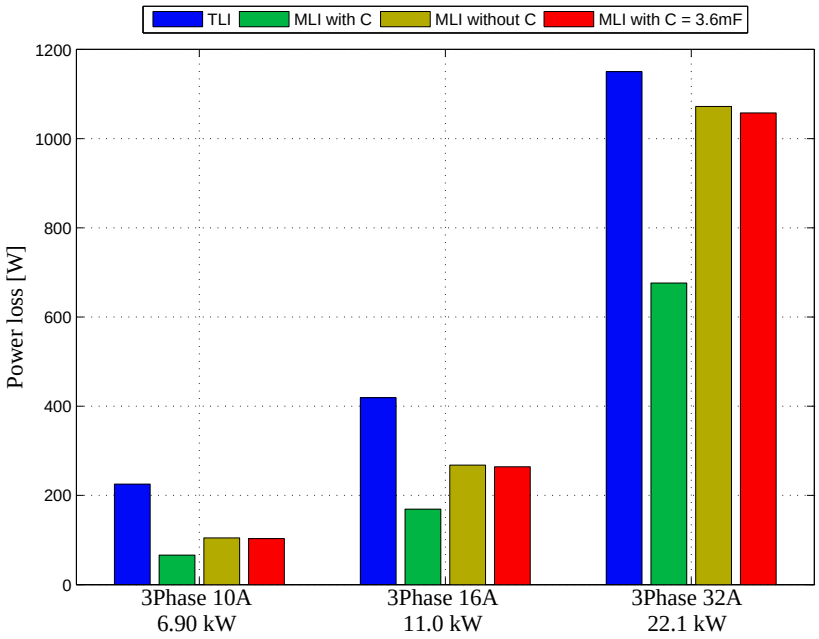

Figure 5.19: Total losses for different charging power

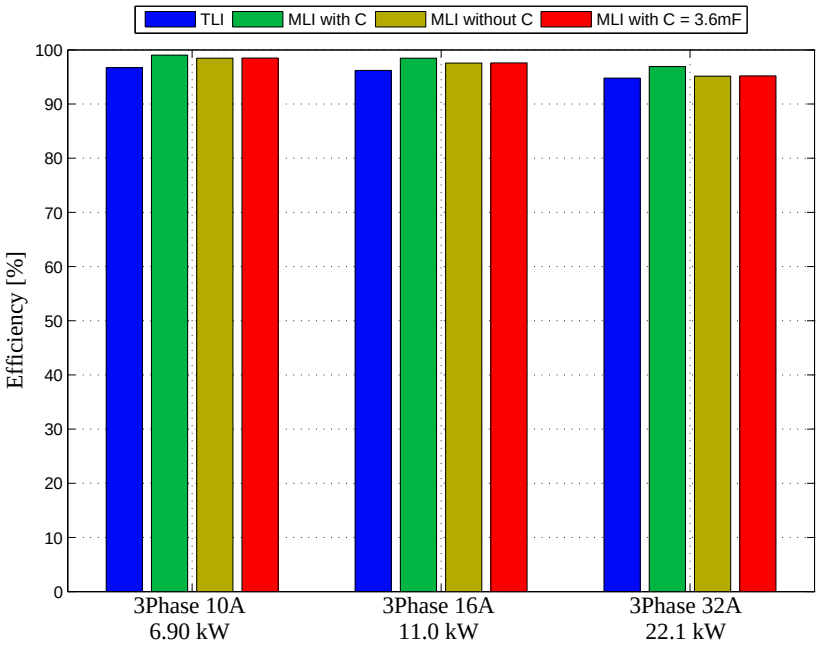

Figure 5.20: Charger efficiency for different charging power

Chapter 6

Drive cycle evaluation

The accumulated energy loss for the battery and the inverter are now analyzed using the NEDC, the FTP75, the HWFET and the US06 drive cycles for the vehicle presented in Table 3.3.

6.1 NEDC

The torque and speed profile for the NEDC drive cycle are shown in Fig. 6.1 and in Fig. 6.2.

The battery and inverter losses for the four different setups are shown in Fig. 6.3 together with the accumulated losses. One can see that the accumulated losses for the TLI drive system becomes the worst ending up at 65 Wh. The MLI that does not have capacitors to filter out the reactive power and harmonic content uses 49 Wh. This is an improvement over the TLI and as can be seen in Fig. 6.13, the inverter losses have been reduced substantially. The battery losses are increased but the sum is reduced. When having a large enough capacitor to the input of the H-bridges the reactive power supply is assumed to be taken from these capacitors instead of the battery. The losses in the battery are then reduced to only 15 Wh instead of 46 Wh. The total losses are then reduced to 18 Wh.

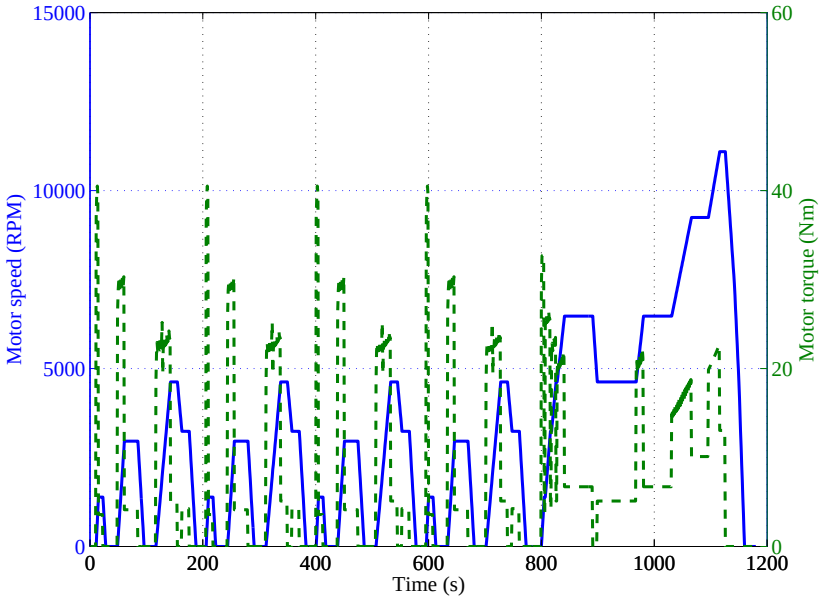

Figure 6.1: The NEDC drive cycle

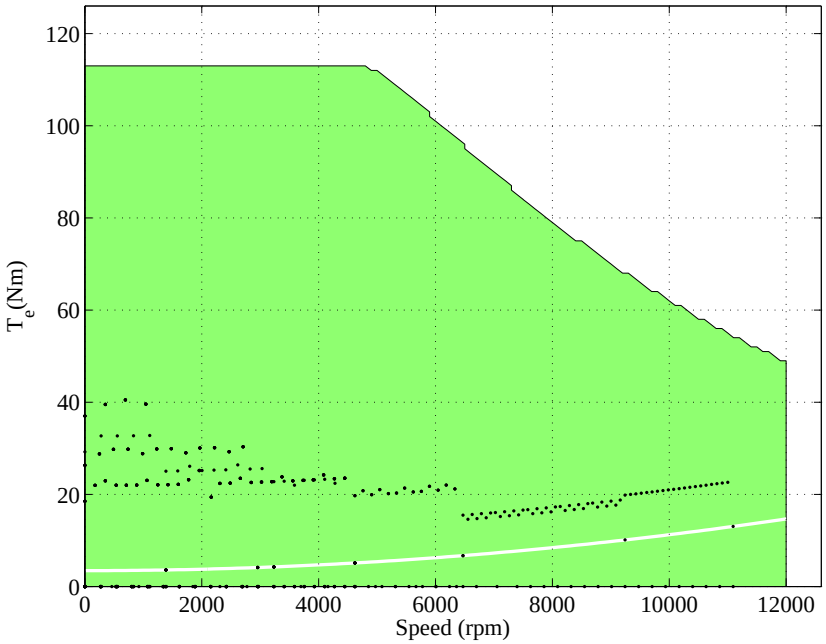

Figure 6.2: Operation points of the electric machine during NEDC

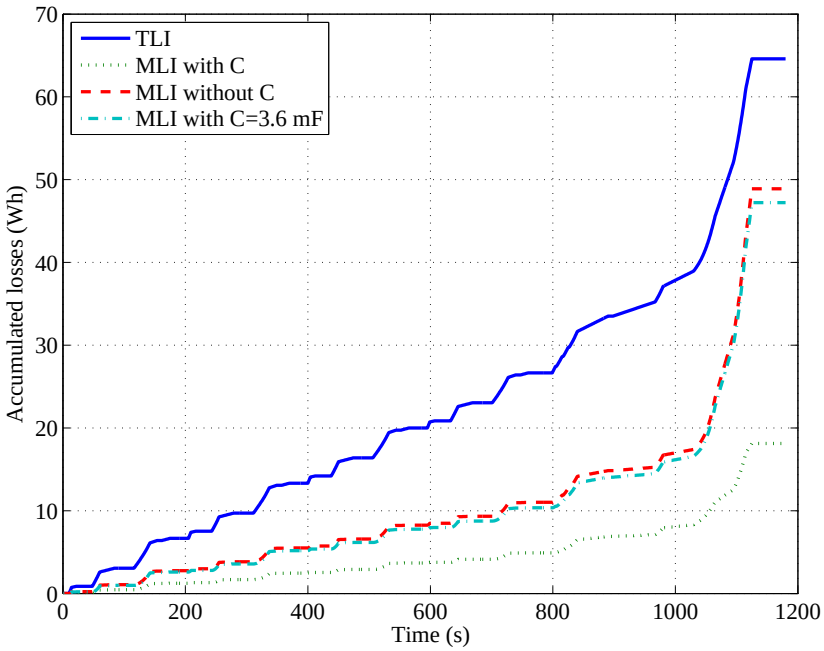

Figure 6.3: Losses during the NEDC driving cycle

6.2 FTP75

The torque and speed profile for the FTP75 drive cycle are shown in Fig. 6.4 and in Fig. 6.5.

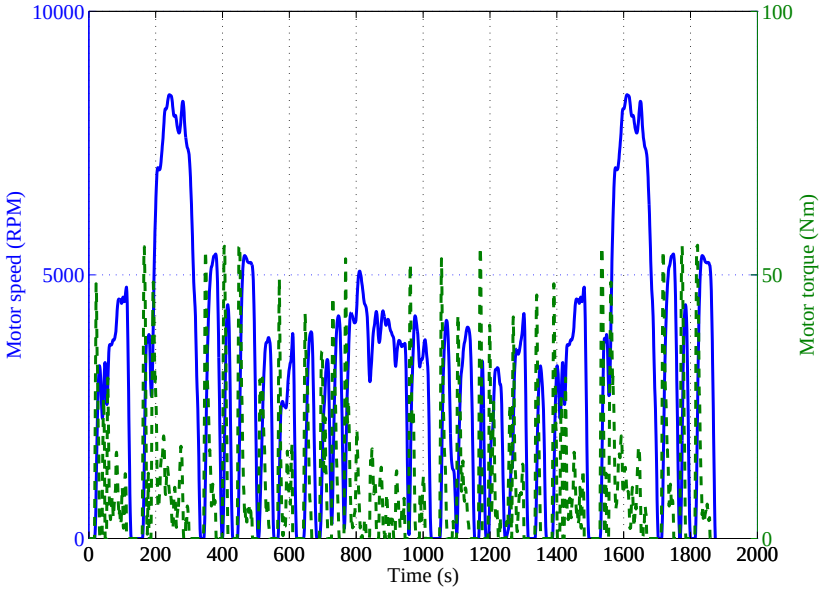

Figure 6.4: The FTP75 drive cycle

The losses for the four different setups are shown in Fig. 6.6 together with the accumulated losses.

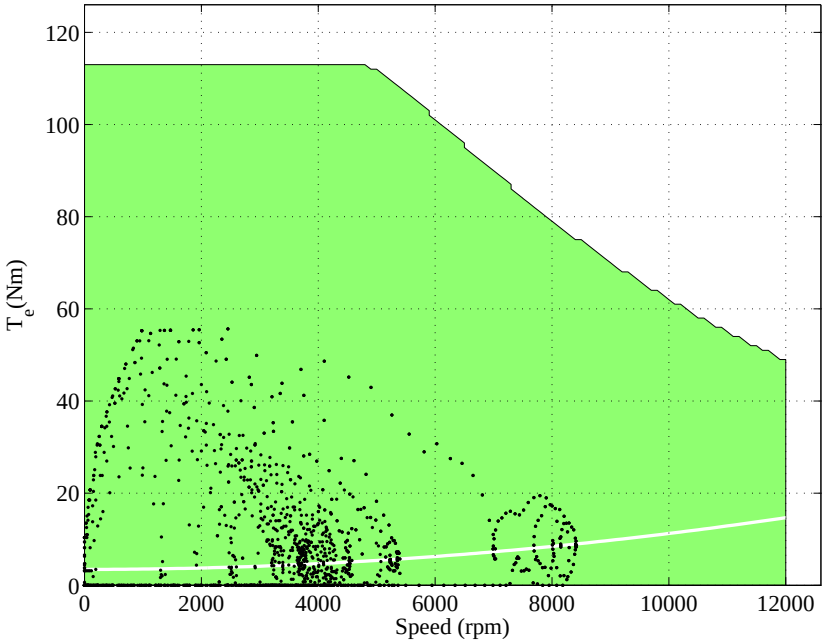

Figure 6.5: Operation points of the electric machine during the FTP75 driving cycle

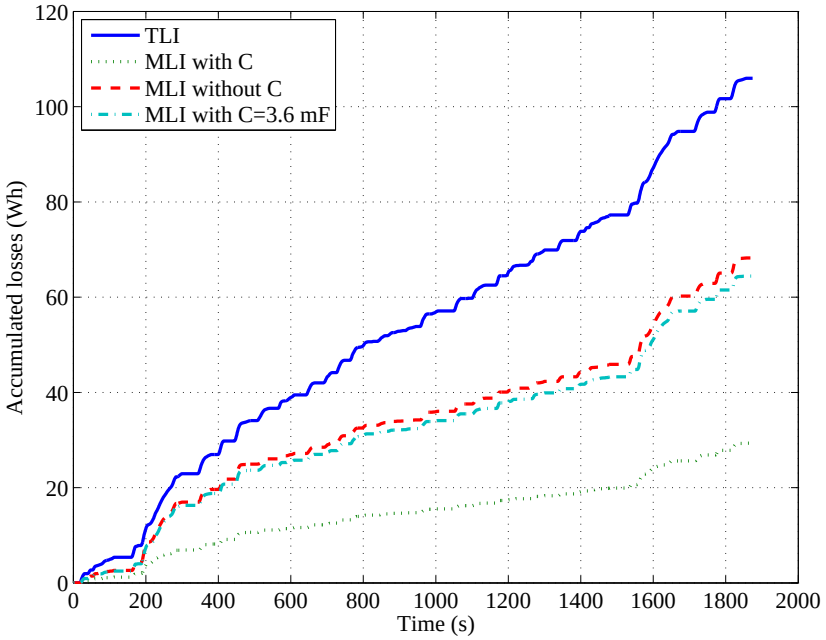

Figure 6.6: Losses during the FTP75 driving cycle

6.3 HWFET

The torque and speed profile for the HWFET drive cycle are shown in Fig. 6.7 and in Fig. 6.8.

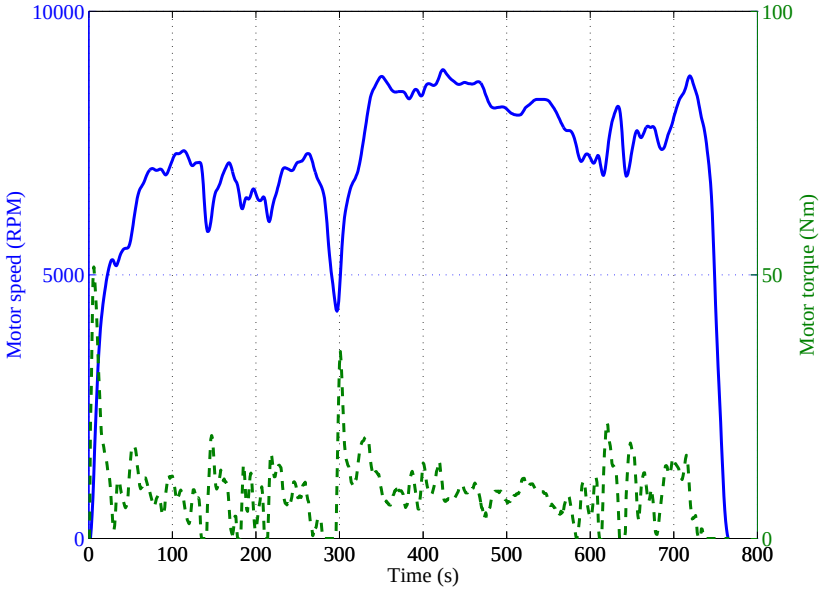

Figure 6.7: The HWFET drive cycle

The losses for the four different setups are shown in Fig. 6.9 together with the accumulated losses.

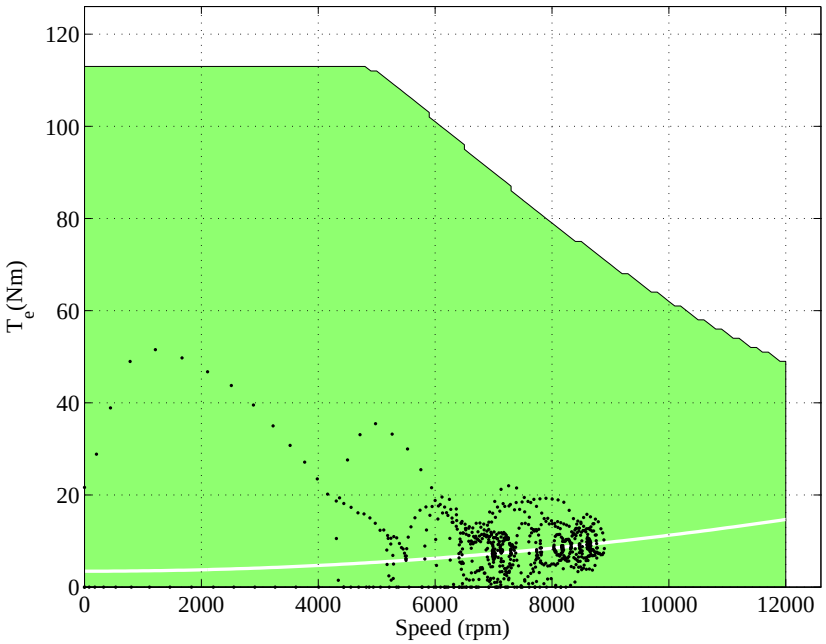

Figure 6.8: Operation points of the electric machine during the HWFET driving cycle

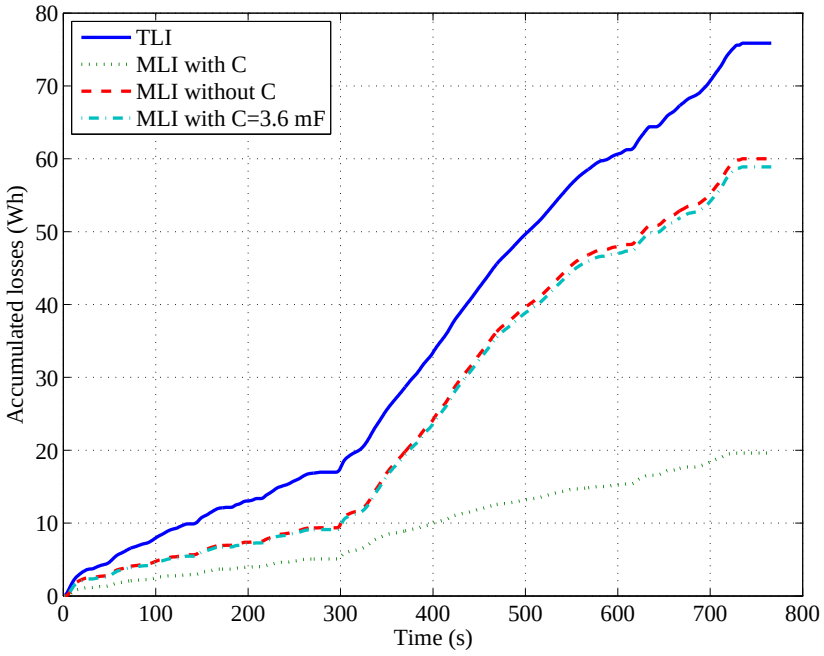

Figure 6.9: Losses during the HWFET driving cycle

6.4 US06

The torque and speed profile for the US06 drive cycle are shown in Fig. 6.10 and in Fig. 6.11.

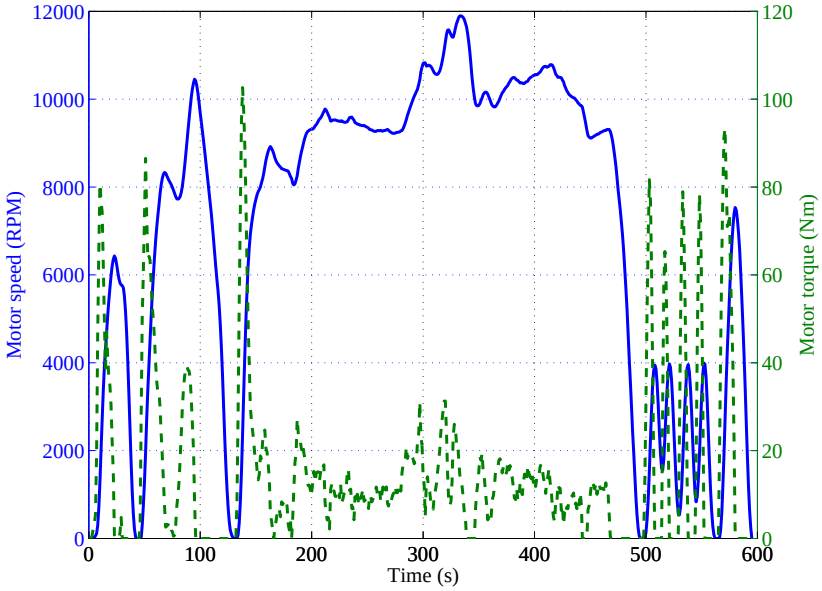

Figure 6.10: The US06 drive cycle

The losses for the four different setups are shown in Fig. 6.12 together with the accumulated losses.

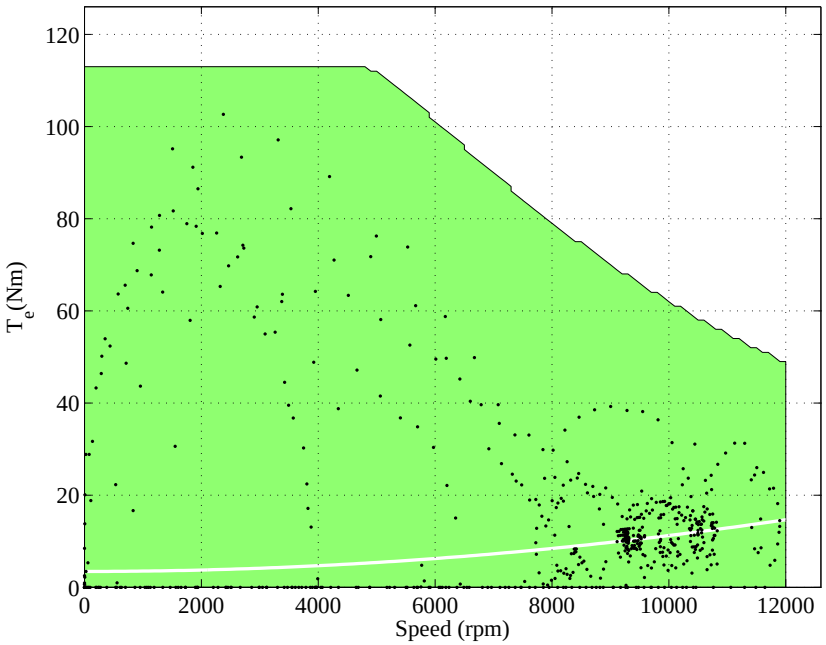

Figure 6.11: Operation points of the electric machine during the US06 driving cycle

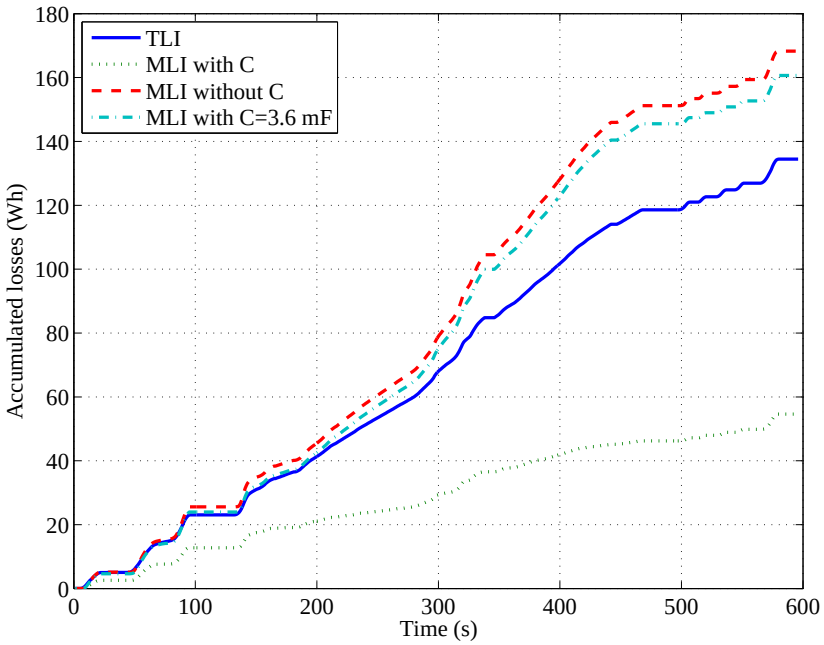

Figure 6.12: Losses during the US06 driving cycle

6.5 Comparison between proposed topology and classical inverter

6.5.1 Propulsion

The accumulated battery and inverter losses for the four drive cycles and the four systems are presented in Table 6.1 and Fig. 6.13 when operating the vehicle with the main machine. It can be seen that the MLI is a beneficial choice compared to the TLI for all drive cycles except the high speed US06. Having filter capacitors of 3.6 mF reduces the losses somewhat compared to not having them at all.

Table 6.1: Accumulated energy loss for inverter and battery when operating the vehicle with the main machine

Drive cycle	TLI	MLI $C = \infty$	MLI $C = 0\ mF$	MLI $C = 3.6\ mF$
NEDC	65 Wh	18 Wh	49 Wh	47 Wh
FTP75	106 Wh	29 Wh	68 Wh	64 Wh
HWFET	76 Wh	20 Wh	60 Wh	59 Wh
US06	134 Wh	55 Wh	168 Wh	161 Wh

The accumulated battery and inverter losses for the four drive trains when using the alternative machine are presented Fig. 6.14. The losses when using the alternative machine are reduced compared to the main machine for the high speed drive cycles US06 and HWFET. The alternative machine has lower magnetisation so less reactive power is needed in the field weakening region, and the high speed losses are reduced. It can also be seen that the case with the input capacitors of 3.6 mF shows a better reduction of the losses compared to the case without the capacitors. This improvement comes from that the alternative machine is a 5 pole pair machine and therefore require a higher frequency, the capacitors therefore becomes more efficient. The MLI with input capacitors of 3.6 mF now shows a loss improvement over the TLI for all drive cycles.

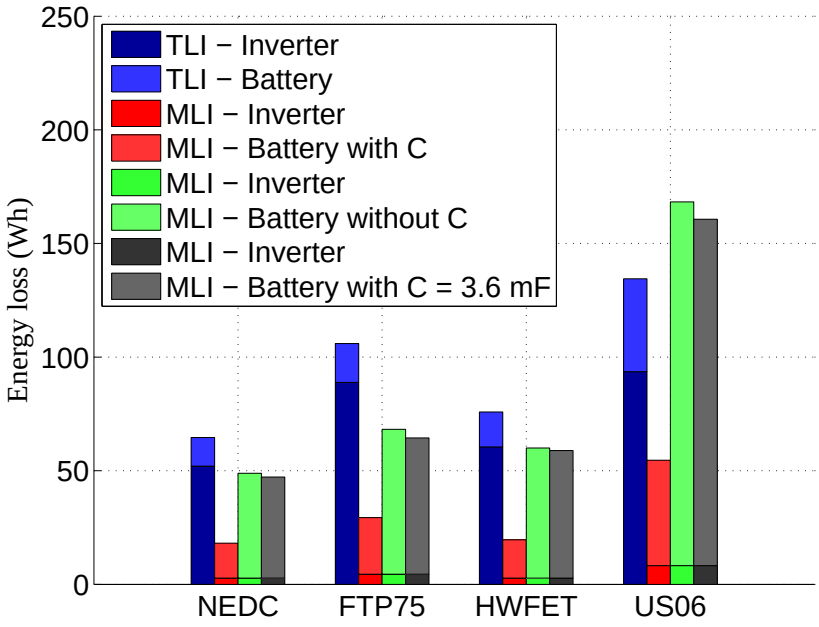

Figure 6.13: Drive cycle losses with main machine

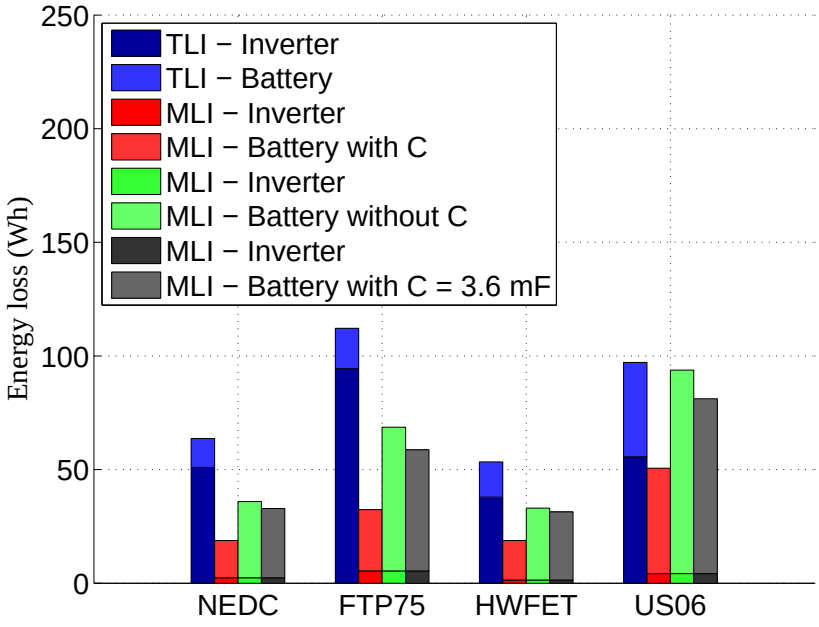

Figure 6.14: Drive cycle losses with alternative machine

Chapter 7

Conclusions

The results show that the multilevel inverter, MLI, has a large potential when used as the propulsion inverter in EVs. It has benefits such as lower EMI, better control over battery management and battery loss distribution. If the possibility to place large capacitors on the input of the H-bridges exists, the drive train losses become lower than the corresponding two-level, TLI, setup for all the drive cycles analysed, especially if the electric machine in the vehicle does not require a large amount of reactive power in the field weakening region. The inverter losses are lowered for all operating points, however the drawback of the MLI is that the battery losses are increased, especially if the input capacitors do not exist. The battery will then supply all the reactive power and harmonic components which is required by the machine and produced by the inverter.

The accumulated losses shown in Table 6.1 show that it is beneficial to use the MLI compared to the TLI. For the NEDC driving cycle the accumulated losses in the battery and the inverter are reduced by 25 % if no input capacitors are used. If on the other hand all the reactive power and harmonic content were supplied by these capacitors the loss reduction would be 72 %. However, these capacitors would be very expensive.

Only for the high speed driving cycle as the US06, the MLI shows a drawback if large input capacitors are not used. The accumulated battery and inverter losses would increase by 25 % when using a MLI without capacitors compared to a TLI. The US06 demands more power due to its higher speeds, and at high speeds the electric machine needs to be controlled with field weakening which requires a lot of reactive power. This reactive power needs to be supplied by the batteries if no input capacitors are available. If the reactive power from the battery is filtered out, the drive system with the MLI becomes the choice with the lowest losses, even at the demanding US06, and shows a loss reduction of 55 %.

Chapter 8

Future Work

This thesis analyses the efficiency perspective of using a MLI in EVs. To be able to verify the possibility of a MLI in EVs the following topics needs investigation.

- Analyse the physical benefits when using a MLI instead of a TLI. Here, cooling design and packaging is a highly important aspect. For instance, there is a need to investigate how beneficial it is to distribute the inverters to the batteries.

- With a MLI the possibility to take out other voltage levels can be made. One level can for example directly supply the 12 V system and the MLI could still make sure that this level is balanced with the remaining levels. The vehicle could then be made cheaper, since no DC/DC converter would be needed. The need for galvanic insulation could on the other hand be a problem and needs further investigation.

- Investigate how the performance of a MLI would be when using more levels. What is the optimum for different drive cycles and car sizes?

- At low frequencies the machine can not operate with selective harmonic elimination due to that the motor current would not be sinusoidal. Investigation about when it is necessary to start using PWM is accordingly needed. Since the MOSFETs has much lower switching losses, it could be beneficial to always use PWM, without increasing the losses very much.

- The MLI has the opportunity to control from which modules the energy should be taken from, it can therefore also be used to control where the losses takes place. If one inverter or battery becomes too hot the

MLI can be controlled to use this level less. Investigation about how this control can be made, and the benefits from it can be of interest.

- If a switch and/or in the MLI malfunctions, and is detected, the inverter can be controlled to keep operating without using that level, making the MLI a fault tolerant system. In vehicles this is a very important feature and investigation about the subject is of great interest.

- Investigation about different modulation strategies is of great importance. Reference [38] and [39] for example, show that space vector modulation is an alternative for MLI and shows good performance.

- Since the MLI can choose from which battery groups the energy should be taken from, it could be beneficial to compose the battery storage from different sorts of batteries and maybe even super capacitors. For very urban drive cycles it could be beneficial to use the super capacitors for acceleration and deceleration, and use the batteries as the average energy supply, reducing the losses.

References

[1] A. Emadi, Y. J. Lee, and K. Rajashekara, "Power electronics and motor drives in electric, hybrid electric, and plug-in hybrid electric vehicles," *Industrial Electronics, IEEE Transactions on*, vol. 55, no. 6, pp. 2237 –2245, june 2008.

[2] R. Roy and J. Ghouili, "Numerical simulation of a multipowered onboard drive train," in *Electrical and Computer Engineering, 2004. Canadian Conference on*, vol. 4, may 2004, pp. 2069 – 2072 Vol.4.

[3] S. Imai, N. Takeda, and Y. Horii, "Total efficiency of a hybrid electric vehicle," in *Power Conversion Conference - Nagaoka 1997., Proceedings of the*, vol. 2, aug 1997, pp. 947 –950 vol.2.

[4] M. Ceraolo, A. di Donato, and G. Franceschi, "A general approach to energy optimization of hybrid electric vehicles," *Vehicular Technology, IEEE Transactions on*, vol. 57, no. 3, pp. 1433 –1441, may 2008.

[5] N. Mutoh, Y. Hayano, H. Yahagi, and K. Takita, "Electric braking control methods for electric vehicles with independently driven front and rear wheels," *Industrial Electronics, IEEE Transactions on*, vol. 54, no. 2, pp. 1168 –1176, april 2007.

[6] D. Gao, C. Mi, and A. Emadi, "Modeling and simulation of electric and hybrid vehicles," *Proceedings of the IEEE*, vol. 95, no. 4, pp. 729 –745, april 2007.

[7] J. Wu, A. Emadi, M. Duoba, and T. Bohn, "Plug-in hybrid electric vehicles: Testing, simulations, and analysis," in *Vehicle Power and Propulsion Conference, 2007. VPPC 2007. IEEE*, sept. 2007, pp. 469 –476.

[8] P.-S. Kim, "Cost modeling of battery electric vehicle and hybrid electric vehicle based on major parts cost," in *Power Electronics and Drive Systems, 2003. PEDS 2003. The Fifth International Conference on*, vol. 2, nov. 2003, pp. 1295 – 1300 Vol.2.

[9] C. Chan, "The state of the art of electric, hybrid, and fuel cell vehicles," *Proceedings of the IEEE*, vol. 95, no. 4, pp. 704 –718, april 2007.

[10] C. Chan and Y. Wong, "The state of the art of electric vehicles technology," in *Power Electronics and Motion Control Conference, 2004. IPEMC 2004. The 4th International*, vol. 1, aug. 2004, pp. 46 –57 Vol.1.

[11] C. Chan and K. Chau, "Power electronics challenges in electric vehicles," in *Industrial Electronics, Control, and Instrumentation, 1993. Proceedings of the IECON '93., International Conference on*, nov 1993, pp. 701 –706 vol.2.

[12] J. Miller, "Power electronics in hybrid electric vehicle applications," in *Applied Power Electronics Conference and Exposition, 2003. APEC '03. Eighteenth Annual IEEE*, vol. 1, feb. 2003, pp. 23 –29 vol.1.

[13] Z. Shen and I. Omura, "Power semiconductor devices for hybrid, electric, and fuel cell vehicles," *Proceedings of the IEEE*, vol. 95, no. 4, pp. 778 –789, april 2007.

[14] S. Haghbin, K. Khan, S. Lundmark, M. Alaküla, O. Carlson, M. Leksell, and O. Wallmark, "Integrated chargers for ev's and phev's: examples and new solutions," in *Electrical Machines (ICEM), 2010 XIX International Conference on*, sept. 2010, pp. 1 –6.

[15] L. Tolbert, F. Peng, and T. Habetler, "Multilevel inverters for electric vehicle applications," in *Power Electronics in Transportation, 1998*, oct 1998, pp. 79 –84.

[16] A. Verma, P. Thakura, K. Jana, and G. Buja, "Cascaded multilevel inverter for hybrid electric vehicles," in *Power Electronics (IICPE), 2010 India International Conference on*, jan. 2011, pp. 1 –6.

[17] D. Graovac and M. Pürschel, "Igbt power losses calculation using the data-sheet parameters," unpublished. [Online]. Available: http://www.element14.com/community/servlet/JiveServlet/download/20553-1-3493/IGBT\%20Power\%20Losses\%20Calculation\%20using\%20the\%20Data\%20Sheet\%20Parameters.pdf

[18] P. Haaf and J. Harper, "Diode reverse recovery and its effect on switching losses," unpublished. [Online]. Available: http://www.fairchildsemi.com/onlineseminars/diodeReverseRecoverySwitchingLosses.pdf

[19] M. Dahidah and V. Agelidis, "Selective harmonic elimination multilevel converter control with variant dc sources," in *Industrial Electronics and Applications, 2009. ICIEA 2009. 4th IEEE Conference on*, may 2009, pp. 3351 –3356.

[20] E. Guan, P. Song, M. Ye, and B. Wu, "Selective harmonic elimination techniques for multilevel cascaded h-bridge inverters," in *Power Electronics and Drives Systems, 2005. PEDS 2005. International Conference on*, vol. 2, nov. 2005, pp. 1441 – 1446.

[21] J. Jose, G. Goyal, and M. Aware, "Improved inverter utilisation using third harmonic injection," in *Power Electronics, Drives and Energy Systems (PEDES) 2010 Power India, 2010 Joint International Conference on*, dec. 2010, pp. 1 –6.

[22] A. Shafiei, A. Momeni, and S. Williamson, "Battery modeling approaches and management techniques for plug-in hybrid electric vehicles," in *Vehicle Power and Propulsion Conference (VPPC), 2011 IEEE*, sept. 2011, pp. 1 –5.

[23] M. Jongerden and B. Haverkort, "Which battery model to use?" *Software, IET*, vol. 3, no. 6, pp. 445 –457, december 2009.

[24] R. Kroeze and P. Krein, "Electrical battery model for use in dynamic electric vehicle simulations," in *Power Electronics Specialists Conference, 2008. PESC 2008. IEEE*, june 2008, pp. 1336 –1342.

[25] M. Duvall, "Battery evaluation for plug-in hybrid electric vehicles," in *Vehicle Power and Propulsion, 2005 IEEE Conference*, sept. 2005, p. 6 pp.

[26] W. Shuanghong, Z. Qionghua, M. Zhiyuan, and Z. Libing, "Implementation of a 50 kw 4-phase switched reluctance motor drive system for hev," in *Electromagnetic Launch Technology, 2004. 2004 12th Symposium on*, may 2004, pp. 518 – 522.

[27] (2013, Feb.) Tesla motors. [Online]. Available: http://www.teslamotors.com/roadster/technology/motor

[28] M. Ehsani, K. Rahman, and H. Toliyat, "Propulsion system design of electric and hybrid vehicles," *Industrial Electronics, IEEE Transactions on*, vol. 44, no. 1, pp. 19 –27, feb 1997.

[29] J. Lindström, *Development of an ExperimentalPermanent-Magnet Motor Drives*. Licentiate Thesis, Chalmers University of Technology, 1999.

[30] J. Hellsing, *Design and Optimization of a Permanent Magnet Motor for a Hybrid Electric Vehicle*. Licentiate Thesis, Chalmers University of Technology, 1998.

[31] I. Khan, "Battery chargers for electric and hybrid vehicles," in *Power Electronics in Transportation, 1994. [Proceedings]*, oct 1994, pp. 103 –112.

[32] L. Tolbert, F. Z. Peng, T. Cunnyngham, and J. Chiasson, "Charge balance control schemes for cascade multilevel converter in hybrid electric vehicles," *Industrial Electronics, IEEE Transactions on*, vol. 49, no. 5, pp. 1058 – 1064, oct 2002.

[33] M. Yilmaz and P. T. Krein, "Review of battery charger topologies, charging power levels, and infrastructure for plug-in electric and hybrid vehicles," *Power Electronics, IEEE Transactions on*, vol. 28, no. 5, pp. 2151 –2169, may 2013.

[34] L. Wang, J. Liang, G. Xu, K. Xu, and Z. Song, "A novel battery charger for plug-in hybrid electric vehicles," in *Information and Automation (ICIA), 2012 International Conference on*, june 2012, pp. 168 –173.

[35] F. Lacressonniere and B. Cassoret, "Converter used as a battery charger and a motor speed controller in an industrial truck," in *Power Electronics and Applications, 2005 European Conference on*, 0-0 2005, pp. 7 pp. – P.7.

[36] D.-G. Woo, G.-Y. Choe, J.-S. Kim, B.-K. Lee, J. Hur, and G.-B. Kang, "Comparison of integrated battery chargers for plug-in hybrid electric vehicles: Topology and control," in *Electric Machines Drives Conference (IEMDC), 2011 IEEE International*, may 2011, pp. 1294 –1299.

[37] K. Ding, K. Cheng, S. Wang, D. Wang, and Z. Shi, "Five-level cascaded multilevel motor driver for electrical vehicle with battery charge management," in *Power Engineering Conference, 2008. AUPEC '08. Australasian Universities*, dec. 2008, pp. 1 –6.

[38] X. Hou, Y. Li, and Y. Liu, "A novel general space vector modulation algorithm for multilevel inverter based on imaginary coordination," in *Power Electronics and Drive Systems, 2003. PEDS 2003. The Fifth International Conference on*, vol. 1, nov. 2003, pp. 392 – 396 Vol.1.

[39] Y. Li, Y. Gao, and X. Hou, "A general svm algorithm for multilevel converters considering zero-sequence component control," in *Industrial Electronics Society, 2005. IECON 2005. 31st Annual Conference of IEEE*, nov. 2005, p. 6 pp.